




Review

# Silica Mesoporous Structures: Effective Nanocarriers in Drug Delivery and Nanocatalysts

Masoud Mirzaei <sup>1,\*</sup>, Malihe Babaei Zarch <sup>1</sup>, Mahdieh Darroudi <sup>2</sup>, Khalilollah Sayyadi <sup>3,4</sup>, Seyed Tahmoures Keshavarz <sup>5</sup>, Jalil Sayyadi <sup>6</sup>, Azadeh Fallah <sup>7</sup> and Hajar Maleki <sup>8,\*</sup>

<sup>1</sup> Department of Chemistry, Faculty of Science, Ferdowsi University of Mashhad, Mashhad 9177948974, Iran; babaie.malihe@yahoo.com

<sup>2</sup> Department of Energy Science and Technology, Faculty of Science, Turkish-German University, Istanbul 10634820, Turkey; m.darroudi@stu.umz.ac.ir

<sup>3</sup> Young Researchers Society, Shahid Bahonar University of Kerman, Kerman 7616913439, Iran; Khalilsayyadi32@gmail.com

<sup>4</sup> Department of Chemistry, Shahid Bahonar University of Kerman, Kerman 7616913439, Iran

<sup>5</sup> Novel Drug Delivery Systems Department, Iran Polymer and Petrochemical Institute, Tehran 14965/115 Iran; Tahmoures.keshavarz@gmail.com

<sup>6</sup> Department of Environmental Health Engineering, Faculty of Health, Zabol University of Medical Sciences, Zabol 9861615881, Iran; jsayyadi59@gmail.com

<sup>7</sup> Department of Chemistry, Payame Noor University of Tehran, Tehran 19395-4697, Iran; Azadehfallah84@gmail.com

<sup>8</sup> Department of Chemistry, Institute of Inorganic Chemistry, University of Cologne, GreinstraÙe 6, 50939 Cologne, Germany

\* Correspondence: mirzaeesh@um.ac.ir (M.M.); h.maleki@uni-koeln.de (H.M.)

Received: 6 October 2020; Accepted: 23 October 2020; Published: 26 October 2020



**Abstract:** The application of silica mesoporous structures in drug delivery and the removal of pollutants and organic compounds through catalytic reactions is increasing due to their unique characteristics, including high loading capacities, tunable pores, large surface areas, sustainability, and so on. This review focuses on very well-studied class of different construction mesoporous silica nano(particles), such as MCM-41, SBA-15, and SBA-16. We discuss the essential parameters involved in the synthesis of these materials with providing a diverse set of examples. In addition, the recent advances in silica mesoporous structures for drug delivery and catalytic applications are presented to fill the existing gap in the literature with providing some promising examples on this topic for the scientists in both industry and academia active in the field. Regarding the catalytic applications, mesoporous silica particles have shown some promises to remove the organic pollutants and to synthesize final products with high yields due to the ease with which their surfaces can be modified with various ligands to create appropriate interactions with target molecules. In the drug delivery process, as nanocarriers, they have also shown very good performance thanks to the easy surface functionalization but also adjustability of their porosities to providing in-vivo and in-vitro cargo delivery at the target site with appropriate rate.

**Keywords:** silica; mesoporous; drug delivery; nanocarrier; nanomaterial; nanocatalysts

## 1. Introduction

Porous nanostructures are a special group of materials that have cavities/porosities at the nanoscale and exhibit different physicochemical features [1]. These properties are determined by their shape [2], size [3], and composition. Compared to uniform particles of the same size, porous nanomaterials have unique properties due to their vacant spaces, including low densities [4–7], large active surfaces [8–10],

low refractive coefficients [11–14], desirable permeabilities [15–17], good selectivity [18–20], and thermal and acoustic resistances [21–23]. The above-mentioned characteristics of porous nanostructures have resulted in the presentation of diverse nanoporous materials, which have attracted the attention of scientists in a variety of fields. The ratio of free-space pores to the total volume of a material is defined as porosity [24,25], which in this category, a pore connected to the free surface of substance is called an open cell [26], and materials with open cells are suitable for use in, e.g., filtration [27], membranes [28], separation [28], and chemical operations, playing roles as catalysts [28] and in chromatography [29]. A pore that is far away from the free surface of a composition is called a closed-cell [30], and these closed cells, while they increase the thermal and acoustic resistance of these materials, as well as reduce their weights, do not contribute to any chemical applications [21–23,31]. Pores come in a variety of shapes and can be spherical [30], cylindrical [32], grooves [33], and hexagonal [34]. A wide variety of porous nanomaterials are available with very diverse properties, structures, and applications. The most useful method for the classification of these materials is to use the diameters of the cavities. Many of the important exclusivities in adsorption and permeation technology relate to these diameters. According to the definition provided by the IUPAC, porous solids are sorted into three basic types based on diameters of their pores: Microporous (<2 nm) [35], silica mesoporous (2–50 nm) [36], and macroporous (>50 nm) [37]. Among these porous solids, mesopores are more efficient than the others due to their large surface areas [38], high porosities [39], tuneable pores [40], excellent thermal properties [41], and mechanical stability [42]. They are used in many different applications, including drug delivery systems (DDSs) [43], catalysts [44], sensors [45], adsorption [46], and separation [47], and are divided into the SBA (Santa Barbara amorphous) [48], MCM (Mobil Composition of Matter) [49], FSM (folding shield mechanism) [50], TUD (Delft University of Technology) [51], and HMS (hollow mesoporous silica) types [52]. In the preparation of silica nanoparticles, different types of precursors can be used depending on whether hardness or flexibility is desired, whether a lipophilic or hydrophilic material is required, and what the density of catalytic active centres on the surface is to be. Since the early 21st century, attempts have been made to make all kinds of silica nanoparticles. By using organic fluids, the structural elements of the structures, and solutions of water and alcohol as solvents, new inorganic substrates with regular structures in nanometre dimensions were prepared. In the late 1990s, various studies were conducted to identify the silica structures and the factors affecting the morphological features, such as temperature and pH, of compositions and solvents. In addition, other compounds, including salts, were used as additives in the production of various types of these materials.

Interestingly, these nanostructures have internal (cylindrical pores) [53] and exterior [54] surfaces that allow selective functionalization for catalytic and drug delivery applications. The main purpose of this review is providing a general knowledge over the recent applications of mesoporous silica as nanocatalyst and carrier for drug delivery. Also, various novel methodologies for preparation of this type of nanocatalyst and their catalytic system up until present time have been provided. Thus, an in-depth study on the catalytic applications, and the usage as nanocarrier for drug-delivery, will be highlighted.

## 2. Synthesis Mechanism Used to Create a Mesoporous Material

The same general synthesis mechanism is used in all meso-structures. Surfactants play the basic roles in the syntheses of porous silica nanoparticles [55]. These structures have hydrophobic and hydrophilic components with different characteristics. The hydrophobic part is dissolved in the nonpolar segment, and the hydrophilic part is soluble in water or polar materials [56,57]. Structures that include hydrophobic and hydrophilic sites are called amphiphilic substances [58]. Many strategies have been introduced to understand mesoporous syntheses. Liquid crystal templating (LCT) is one of the most well-known methods. Surfactants play a crucial role in LCT [59]. In very low concentrations, these materials take the form of soluble monomers. As their concentrations are enhanced, the molecules accumulate in aqueous solutions, and isotropic spherical and tubular micelles form, reducing the free energy of the system [60]. At even greater concentrations, hexagonal compositions are created from the surfactants. These structures act as templates, and when inorganic precursors are added, they are placed on these templates [61]. Most inorganic compounds have an area with a negative charge,

allowing them to interact electrostatically with the positive heads of the surfactants. When these materials are placed on the surface, the compression stage is reached, and the integrated framework of the inorganic component is established on the surface of the surfactants. Finally, when the surfactants are removed, a mesopore is created [59].

It should be pointed out that the morphology of a silica mesopore can be affected by various factors, including the surfactant and co-surfactant used, source of the silica, temperature, alcohol used, and pH.

### 3. Factors in the Synthesis of a Mesoporous Material

#### 3.1. Surfactant

Generally, surfactants act as templates and have key roles in the syntheses of mesoporous materials. These surfactants can be divided into four groups, including (1) ionic surfactants, which contain sulphonated compounds with the general formula  $R-SO_3Na$  and sulphated compounds with the general formula  $R-OSO_3Na$  [62]; (2) cationic surfactants, which commonly contain alkali hydrophilic and methylammoniums such as CTAB (cetyltrimethylammonium bromide ( $C_{16}H_{33}N(CH_3)_3Br$ )) and hexadecyltrimethylammonium (HDTMA) [63]; (3) non-ionic surfactants, which, when dissolved in solvents, do not decompose into ions [64]; and (4) amphoteric surfactants, which exhibit characteristics of ionic and non-ionic surfactants simultaneously, e.g., phospholipids. Different aspects, such as chain length [65], chain structure [66], pH [67], being used as an electrolyte [68], and temperature [69], affect the efficiency of these kinds of surfactants. For instance, in order to prepare mesoporous materials for different purposes having pores of uniform size and with diameters larger than 5 nm, the active surface of Pluronic P123 ( $EO_{20}PO_{70}EO_{20}$ ) (a non-ionic surfactant), a three-dimensional polymer, can be used as a template in an acidic environment. The sizes of the pores and the wall thicknesses can be changed by enhancing the hydrophilic head of the surfactant [55]. Niu et al. [69] developed a mesoporous core-shell with two modes using amphiphilic copolymers of (polystyrene-*b*-poly (acrylic acid), PS-*b*-PAA) and CTAB as co-templates (Figure 1). As can be seen in Figure 1, the PAA copolymer, by attaching to the CTAB micelles, initially creates the micelle composition. Then, the TEOS (tetraethyl ortho-silicate) is placed on the micelle composition. Subsequently, through the self-assembly actions of the CTAB and TEOS, a core-shell mesoporous material with a two-mode structure is obtained. Wiesner et al. [70] have reported the synthesis of aminated-mesoporous particles with adjusted particle sizes. Contrary to findings in the previous work, the presence of ethyl acetate in an ammonia solution increased the amount of aminosilane connected to the mesoporous material greatly, while its ordered shape remained intact. Recently, gemini surfactants (GSs) have been investigated as versatile templates for the synthesis of silica mesopores. GSs have hydrophobic heads and interconnected spacers between or near the hydrophobic chains, allowing convenient aggregations in solution [70]. Li et al. used GS with 14-2-14 molecules to prepare hollow mesoporous silica (HMS) [71]. In summary, surfactants have essential roles in the polymerization of silicate species to form their respective mesoporous silicate nanoparticles. Self-assembly in solution produces desirable results for various applications.

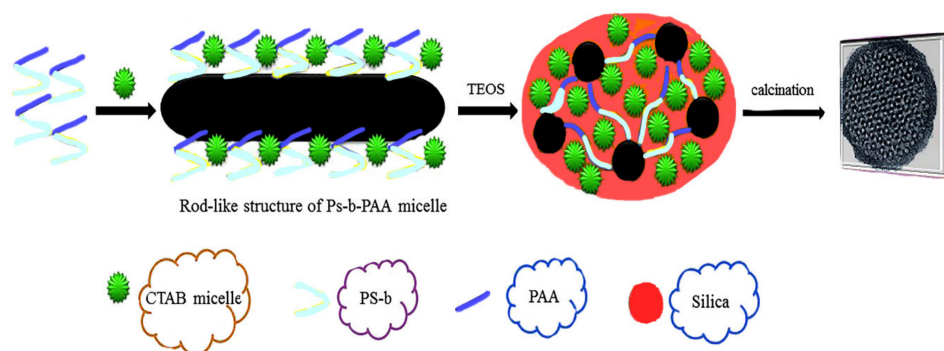


**Figure 1.** Synthesis of a silica mesopore using cetyltrimethylammonium bromide ( $C_{16}H_{33}N(CH_3)_3Br$ ) (CTAB) and (polystyrene-*b*-poly (acrylic acid) (Ps-*b*-PAA) as amphiphilic.

### 3.2. Co-Surfactants

Co-surfactant materials, such as alcohols, not only significantly affect the ductility and size of the pores, but also, as their concentrations are increased, diminish the percentage of spherical shapes present in the respective mesoporous materials. Hence, they control the shape and size of the particles, and in their absence, amorphous particles will be formed having different and disordered sizes [72,73]. Surfactant materials, such as the anionic/cationic surfactant, ionic liquid, solvents, and so forth, that are used in the fabrication of mesoporous materials, can also be used in *co*-surfactant roles with changes in their morphology. For instance, Zhang et al. [74] suggested an ionic liquid/copolymer system for the synthesis of zirconium loaded inside the pores of mesoporous-microporous silica nanoparticles. The interactions between NTA (*N*-tributylamine acetate (ionic liquid)) and P-123 (co-polymer) and a change in the pH resulted in diverse structures with spherical and branch morphologies. Interestingly, the amount of alcohol serving as a *co*-surfactant can determine the final structure of a *meso*-silica. Stevens et al. [75] used butanol as *co*-surfactant for the syntheses of hexagonal SBA-16 and an array of hexagonal SBA-15 mesopores and studied its effects. Adding it to the reactions increased the sizes of the SBA-16 and SBA-15 pores, thus improving their catalytic and drug delivery performances. Yang et al. [76] showed that in acidic conditions, pore size, thermal stability, cavity volume, and surface area are enhanced by an appropriate molar ratio of a *non*-ionic (P123)/ionic (SDS: sodium decylsulphate) *co*-surfactant system. Therefore, *co*-surfactant can act as a complementary role in the manufacture of mesopore nanoparticles in terms of controlling the morphology and size of particles.

### 3.3. Silica Source

Oligomeric precursors and silicone monomers are commonly used for the fabrication of mesoporous materials, thus preventing irreversible polymerization in acidic conditions. Precursors such as colloidal solutions, sodium silicates, and organosilanes like tetraethyl ortho-silicates can be used for the syntheses of ordered mesoporous materials [74]. Sodium metasilicate ( $\text{Na}_2\text{SiO}_3$ ), when used as a precursor, produces small oligomers upon acidification. The tetramethyl ortho-silicate (TMOS), Tetraethyl orthosilicate (TEOS) tetrapropyl ortho-silicate (TPOS), trimethoxysilane (TMS), tetrabutoxysilane (TBOS), and other typical silica-based precursors are used as mesoporous precursors [75]. Among these precursors, TMS is the fastest in the formation of silicate mesoporous structures. It should be noted that since the porous meso-structures produce slowly, TBOS should also be added slowly [76]. Although other factors, such as pH and the molar ratio of surfactant to silica, affect the syntheses of meso structures, the key roles of silicate sources cannot be ignored. Tang et al. [77] reported the preparation of spherical silica mesoporous via the use of sodium silicate and TEOS under acidic conditions, producing pore sizes in the ranges of 1 to 3.5 nm and 2 to 10 nm, respectively. They demonstrated that the mesoscopic material should be synthesized with fumed silica at a temperature of 850 °C, whereas if the TEOS precursor is used at 750 °C, the mesoporous structure will collapse. The wall thicknesses of the porous materials obtained via these two precursors are the same under identical conditions [77]. However, despite being formed under the same conditions and having walls of equal thickness, they have different thermal stabilities coming from other silicate sources [77].

### 3.4. Temperature

The final properties of mesoporous materials depend mainly on the temperature under which they were created. Mesoporous materials are synthesized at temperatures between 10 to 130 °C, with 25 °C being considered reasonable. The critical micelle temperature (CMT) and the cloud point (CP) are two factors to consider in terms of the temperature [76]. Typically, the selected temperature should be higher than the CMT of the surfactants. For cationic surfactants, CMTs are relatively low. Under these conditions, the rate of accumulation of surfactant temptation decreases with decreasing synthesis temperatures. As a result of this process, high-quality mesoporous materials will be achieved. However, if a *non*-ionic surfactant is utilized as a template, the reaction temperature should be high

due to increased CMT [76]. In the preparation of SBA-15, the synthesis temperature needed for the complete dissolution of the surfactant and the CMT is slightly higher than the ambient temperature. It lies within the range of 40–35 °C [78]. Hence, the diameters of the SBA-15 pores change according to the conversion conditions. In the range of 40–90 °C, there are micropores in the system, and all types of pores have been observed at temperatures of more than 100 °C. Hence, by increasing the temperature, the cavity sizes grow and the thickness of the walls is reduced in SBA-15 mesoporous materials, thus reducing the fraction of cavities that are micropores [78]. The CP is the point at which liquid–liquid phase crystal separation occurs directly on the EO (ethoxy) chain in block copolymers. Therefore, any change in this important point should be considered in the synthesis of silicon *meso*-structures. If the CP decreases, then the lengths of the EO hydrophilic chains will decrease, while the lengths of these chains will increase with increasing CP. Hence, the length of the EO chain varies directly with the CP. In addition, enhancing the CP creates different geometric structures, ranging from lamellar to cubic. A parameter called the critical packing parameter (CPP) is involved in their construction [79]:

Therefore, based on the CMT and CPP mechanisms, we can determine the formation of mesoporous nanostructures and their shapes.

### 3.5. Solvents

Solvents also affect the synthesis of mesoporous materials and alter the shape of the particles. In this regard, the most effective and frequently used solvent is different types of alcoholic solvents. For instance, alcohols with high molecular weights and low evaporation rates have less influence on the shape and morphology of mesoporous materials [78]. On the other hand, alcohols increase the formation and change the sizes of the pores. Commonly, ethanol, propanol, butanol, and pentanol are used in the preparation of mesoporous materials. It should be noted that ethanol sometimes causes the collapse of mesopores' spherical shapes [78]. Alcohols, as solvents, can also alter the channel rotations of mesoporous materials. For instance, Yano et al. have synthesized mesopores with cavity sizes of 10 to 1000 nm via making changes in the ratio of alcohol to water [80].

Furthermore, solvents can also play a vital role in the removal of surfactants in the final step of the synthesis. Cauda et al. prevented the agglomeration of synthetic mesopores by removing surfactants with a solvent containing high-boiling-point alcohol [81]. Lebedev et al. added alcohol as a solvent during the growth of radial MCM-48 to help in growing its cylindrical pores [80]. Alcohols, in addition to their roles as solvents, can also be used as *co*-solvents during syntheses [82]. Alcohols with larger chains make it possible to move to a new phase after a previous phase. Agren et al. reported establishing a new lamellar phase after the hexagonal phase in MCM-41 after adding hexanol [83–87]. Grun et al. added ethanol to the initial solution used by Agren et al. [87] instead of hexanol [88]. Their results indicated that spherical mesoporous silica was present. Qianjun et al. reported the effects of 2-alkanols on the morphologies and sizes of mesoporous materials. They succeeded in showing that in comparison with 1-alkanols, 2-alkanols, such as ethylene glycol (EG), resulted in the formation of particles of greater size and more ordered structural morphologies [84].

### 3.6. pH

Typically, mesoporous materials are prepared in an acidic or alkaline environment. Neutral solutions are not suitable for these types of syntheses since, under neutral conditions, the rate of polymerization and transverse bonding is very high, resulting in the fabrication of a disordered silicate skeleton [85]. To overcome this problem, fluorine catalysts can be used in the syntheses of ordered solids under a neutral pH by adjusting the rate of hydrolysis and condensation of the silicate precursor [86,87]. In an alkaline medium with the pH ranging from 9.5 to 12.5, the polymerization and creation of reversible networks of silicate species are possible. Hence, the above properties have led to the use of silicate precursors, such as colloidal solutions, Na<sub>2</sub>SiO<sub>3</sub>, and TEOS [63]. During the synthesis, the pH changes. At the beginning of the reaction, due to the hydrolysis of silica, the pH decreases and then slightly increases as the components of the silicate species condensate [63]. A similar process occurs in strongly acidic environments since

mesoporous design is less dependent on pH, reaction reversibility, and temperature [88]. As the pH decreases, the rate of synthesis of silica mesopores increases. High concentrations of acidic catalyst increase the rate of precipitation of the silica species. Strong acids, such as HCl, HNO<sub>3</sub>, HBr, and H<sub>2</sub>SO<sub>4</sub>, can be used as catalysts. In some cases, weak acids, such as H<sub>3</sub>PO<sub>4</sub> and CH<sub>3</sub>COOH, are applied. When HCl is utilized as a catalyst, the pH of the system dips below one, whereas, as mentioned earlier, when there is a higher concentration of acid, the product does not reach the desired quality [88]. In general, the precipitation of mesoporous materials in the pH range 1–2 is strongly reduced, which can be related to the presence of an isoelectric point in the silicate source in this range. Since the common route for the synthesis of a mesoporous material is the sol-gel pathway, pH plays an important role.

In the sol-gel method, hydrolysis and condensation processes are used to construct mesoporous nanostructures [89]. Organic compounds are integrated into the inorganic matrix of the mesoporous silica materials [90]. The presence of these organic compounds can then help in the formation of the final product through catalytic effects and improvements in the hydrolysis-condensation reactions. Depending on the nature and number of the organic groups that enter into the system, highly porous meso-structures can be achieved, even with heating [89]. The routes to the mesoporous nanostructure used by the sol-gel method under acidic and basic conditions are shown in Figure 2. In the first step, the acidic/basic silicate precursor is observed, which leads to the generation of a silanol group (creation of sol). In the next step, the silanols react together (condensation), and the gel structure is established by realizing the H<sub>2</sub>O or alcoholic by-products. A wet gel is obtained at this stage, which is ultimately converted into the original gel structure through drying and calcination process. In fact, under acidic conditions, the rate of nucleation determines the rate of the process. Due to the formation of a high concentration of the silanol groups, the final step is hydrolysis. Generally, hydrolysis in the presence of a base catalyst is faster than in an acid catalyst because the base prevents the agglomeration of the sol particles [91]. Therefore, hydrolysis and the condensation of silicate precursors can be considered as the key stage of the meso-structure's preparation method [91]. McCormick et al. showed that a low concentration of an acid catalyst, in addition to being a self-inducing stimulus, is required to begin the reaction [92].

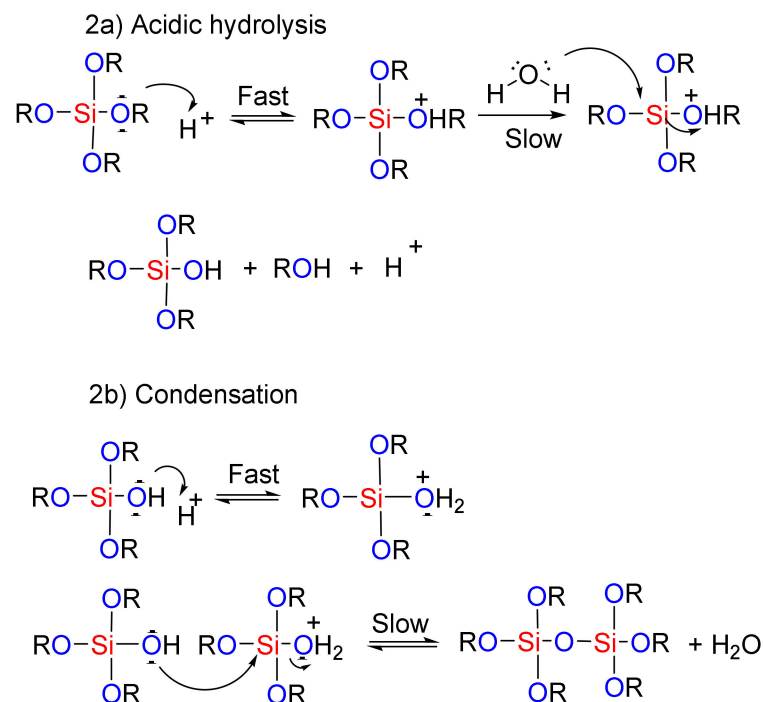
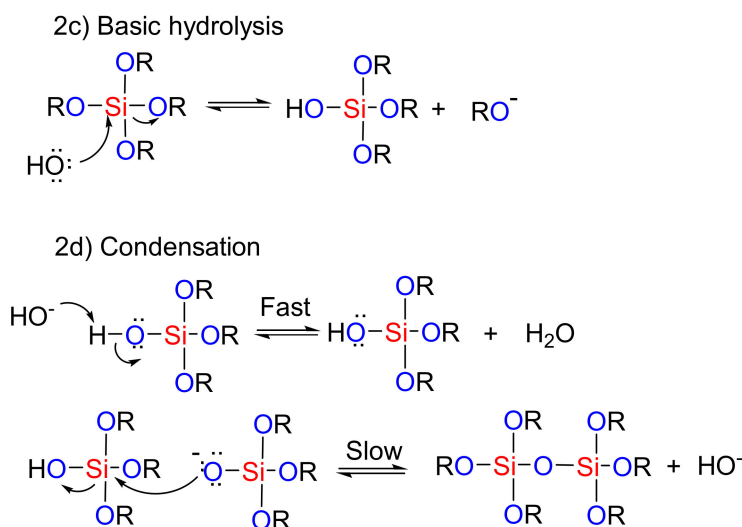


Figure 2. Cont.



**Figure 2.** The role of acidic and basic catalysts in the sol-gel process used for the preparation of mesoporous materials.

#### 4. Catalytic Applications of Mesoporous Silica Materials

In recent years, catalytic applications of mesoporous materials have been explored due to their adjustable pore sizes, biodegradability, and ease of modification with various functional groups. They are very much considered for organic syntheses and the removal of organic dye pollutants. In the following sections, an update from literature is given regarding the recent advances of mesoporous silica-based materials for catalytic applications.

##### 4.1. Removal of Organic Dyes

Large amounts of toxic pollutants, including dyes and heavy metals, have considerable environmental consequences, so the removal of even small amounts of these hazardous compounds is crucial [93]. Many methods, such as separation [94], oxidation/reduction [95], ion exchange [96], adsorption [97], membrane [98], and biological [99] methods, have been developed by researchers over the past decade. Among these methods, the adsorption process is of great interest due to its greater efficiency and simplicity [100]. Organic dyes are dangerous sources of industrial wastewater and come from textiles, dyestuffs, papers, plastics, and cosmetics. Their presence in water endangers humans and plants [101]. For example, Sudan Red (RS) and its derivatives have high levels of toxicity and carcinogenicity, even at low concentrations. Considering that most organic dyes have aromatic structures, they are resistant to dye-removal reactions, although their toxicities are reduced during such reactions [102]. A large number of nano-adsorbents, such as active carbon [103], zeolite [104], nanoclay [105], and an imprinted molecular polymer [106], are used to remove organic dyes from aqueous solutions but have a low adsorption capacity. Therefore, it is necessary to find novel nano-adsorbents that will eliminate the effects of these contaminants and control them at maximum adsorption capacity. To date, nanostructures have been shown to be superior at removing toxic and harmful organic dye compared to other adsorbents, which has made them extremely valuable. Mesoporous materials are one of the most extensively investigated silica nanomaterials because they are excellent adsorbents due to their high pore volumes, large surface areas, and adjustable pore sizes [107]. Like any other adsorbent materials, silica nanoparticles can serve in the effective removal of organic pollutants, e.g., methylene blue (MB) [108], methyl orange (MO) [109], methyl red (MR) [110], malachite green (MG) [111], and everzol blue (EB) [112].

Mesoporous materials can be good candidates for this purpose because they have large surface areas, adjustable cavity sizes, and very high adsorption capacities [107]. The modification and functionalization of mesoporous materials via various functional groups, such as  $-\text{NH}_2$ ,  $\text{COOH}$ ,

and SH and their placement on active sites result in the easy removal of dye pollution [113]. Veisi et al. reported high catalytic activity on the part of magnetic silica nanoparticles in reducing the organic dyes 4-nitrophenol (4-NP), rhodamine B (RhB), and MB (Figure 3) [114].

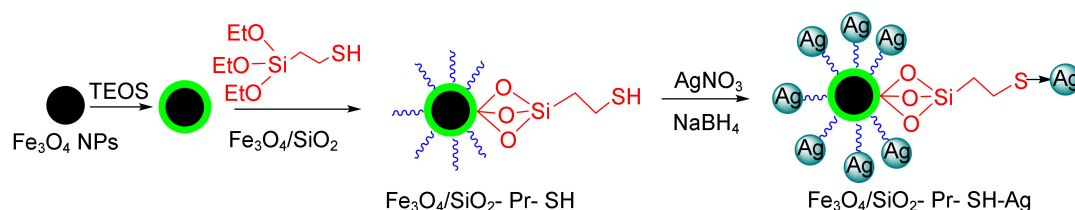


**Figure 3.** The reduction of 4-nitrophenol (4-NP) and rhodamine B (RhB) using the magnetic  $\text{Fe}_3\text{O}_4/\text{SiO}_2$ -Pr-SH-Ag nanocatalyst.

In another study, Song et al. reported on the synthesis of the SBA-15/polydopamine (PDA)/Ag nanocomposite [115]. They showed that the tested nanocomposite degraded 4-NP and MB without decreasing its catalytic activity (Figure 4). Ho et al., removed acid blue 25 and MB using modified MCM-41 with amine and carboxylic acid groups, respectively. Their results showed that there are base–acid interactions between these dyes and the modified mesopores with absorption capacities of  $256 \text{ mg g}^{-1}$  (acid blue 25) and  $113 \text{ mg g}^{-1}$  (MB) [115].

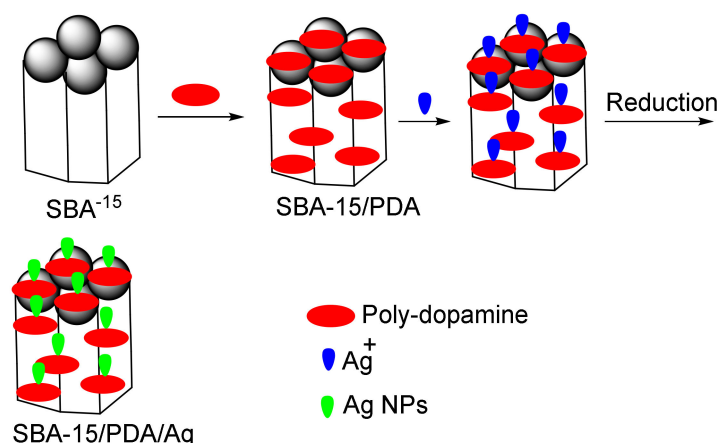


**Figure 4.** The removal of organic acid blue 25 and methylene blue (MB) via the SBA-15/PDA/Ag nano-adsorbent.

## 4.2. Organic Synthesis

### 4.2.1. Oxidation Reaction

In mesoporous materials, the transition metal is grafted onto the framework to introduce redox properties, which are devoid of oxidant activity. Some transition metals could be introduced to occupy the vacant positions within the mesoporous silica framework.

Zhang et al. synthesized tungsten-containing functionalized MCM-41 and employed it in the desulphurization reaction of dibenzothiophene (DBT). The results established that the mesoporous structures were well-preserved after the introduction of the tungsten species into the mesoporous materials [116]. These materials showed a good dispersion of the W species and formed an efficient and highly recyclable catalyst for the removal of dibenzothiophene (Figure 5). The characterization results showed that the mesoporous structure of MCM-41 was maintained after the introduction of the W species. These catalysts showed homogeneous dispersions of the W species in the mesoporous material and excellent catalytic activity in the removal of sulphur-containing compounds. The sulphur content in model oil can be reduced from 500 to 0 ppm with the low usage of an oxidant in 30 min. In the reaction, no organic solvents were added as extractants, and the mesoporous elements



of W-MCM-41 acted not only as absorbents to absorb the sulphur-containing compounds but also as active sites to activate  $\text{H}_2\text{O}_2$  to oxidize the sulphur compounds and convert them to sulphones. The oxidative reactivity of the sulphur-containing compounds decreased according to the following order: 4,6-DMDBT (4,6-dimethyldibenzothiophene) > DBT > BT (Benzothiophene) > DT (Dithiophene). In addition, it was possible to recycle the oxidation system nine times without a significant decrease in activity. Moreover, according to the GC-MS analysis of the oxidation products, a mechanism was proposed for the investigation of the absorptive oxidation process occurring between W-MCM-41 and sulphur-containing compounds [116].

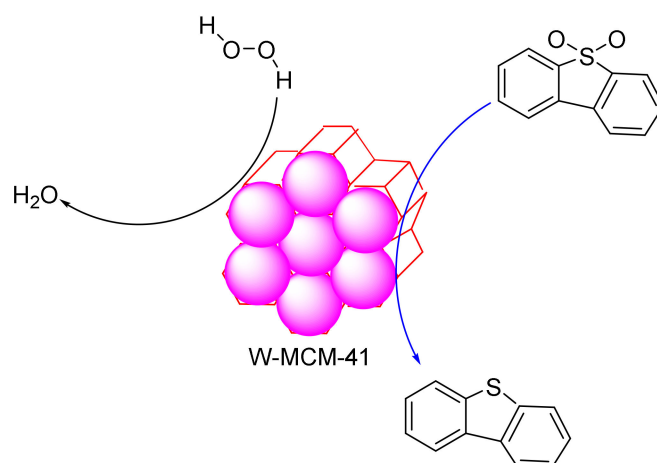


**Figure 5.** The desulphurization reaction of dibenzothiophene on W- MCM-41 (Mobil Composition of Matter No. 41) mesoporous silica.

Also, Tuong et al. reported the solvent-free oxidation of benzyl alcohol to benzaldehyde by iron-chloride immobilized on SBA-15 (SIL- $\text{FeCl}_3$ ) (Figure 6). The SIL- $\text{FeCl}_3$  revealed higher catalytic activity in terms of the effective solvent-free oxidation of benzyl alcohol to benzaldehyde when using the oxidant. This mesoporous catalyst was easily recovered and reused without a significant loss in its activity and selectivity, leading to its potential application in an *eco*-friendly synthesis of chlorine-free benzaldehyde [117].

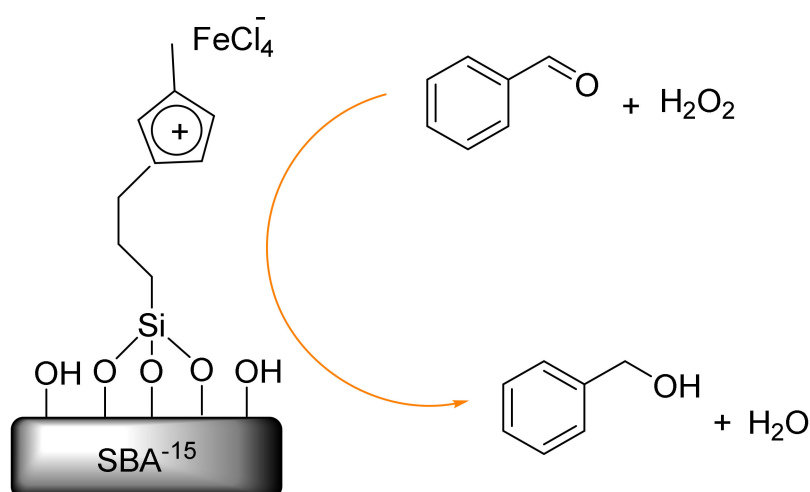


**Figure 6.** The oxidation of benzyl alcohol to benzaldehyde on Santa Barbara amorphous (SBA)-15 (SIL- $\text{FeCl}_3$ ).

Furthermore, Uson et al., reported a novel-sized Pt-decorated SBA-15 rod catalyst functionalized with the tetrakis (hydroxymethyl) phosphonium chloride group (THPC) as both a stabilizer and

reductant in the mesoporous catalysis of *n*-hexane through a facile synthesis method under oxidation, having observed excellent stability and high activity (Figure 7) [118].

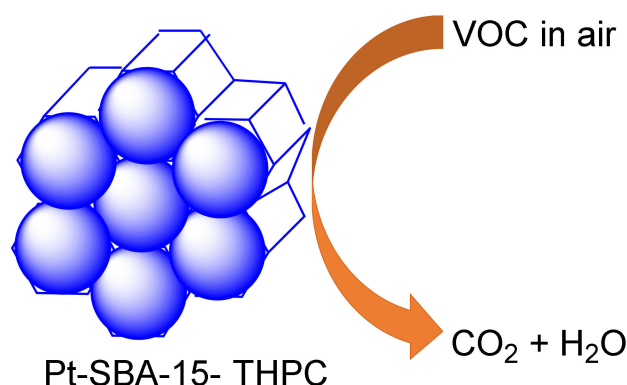


**Figure 7.** The in-situ generation of ultra-small Pt nanoparticles on mesoporous silica rods in high-activity mode in the oxidation of *n*-hexane.

#### 4.2.2. Ring-Opening Polymerization

According to the article published by Cruz et al., a mesoporous, silica-coated Fe core-shell nanoparticle was synthesized via a surfactant template sol-gel method utilizing magnetic nanoparticles (MNPs) stabilized with nucleation seeds exhibiting superparamagnetic behavior [119]. The magnetic behavior and adsorptive properties of these nanoparticles show that these MNPs are appropriate candidates for supporting catalyst preparation via titanium immobilization achieved through post-synthetic procedures. The synthetic parameters are controlled in order to obtain high-quality, core-shell, stable, and biocompatible magnetic mesoporous nanoparticles (MMNPs), which were used to help to prepare heterogeneous catalysts for the ring-opening polymerization of  $\epsilon$ -caprolactone ( $\epsilon$ -CL) in an aqueous and organic medium with excellent activity.

Since this titanium catalyst showed excellent activity for the ring-opening polymerization of  $\epsilon$ -CL, it could also be used under similar conditions. Electrochemical measurements verified Fe (III)'s electron reduction process in magnetite with diverse coordination environments, which could be useful for fast and simple electrochemical measurements of the growth of a silica layer and the complete coating of MNPs [119].

#### 4.2.3. Synthesis of Dimethylcarbonate

Cui et al. reported flowerlike MgO in the synthesis of dimethylcarbonate (DMC) by a meso-SiO<sub>2</sub>, which was coated on Fe<sub>2</sub>O<sub>3</sub>, MgO, an SnO nanosphere, Co<sub>3</sub>O<sub>4</sub>, and nanowire through a simple solution method [120]. In the paper, low-cost synthesis strategies for both nano- and meso-SiO<sub>2</sub> using mesoporous SiO<sub>2</sub> were reported. They found that the meso-SiO<sub>2</sub> coating with its tetrahedral geometry can form a layer to bind and cover the nano building blocks. The silica coating dramatically improved the structural stabilities of several types of nanostructures, including flowerlike nanomaterials (Fe<sub>2</sub>O<sub>3</sub>, MgO), hollow spheres (SnO), nanowires, and nanosheets (Co<sub>3</sub>O<sub>4</sub>). The results showed that a coating of meso-SiO<sub>2</sub> is an ideal method for showing that mechanic stability leads to the remarkable catalytic stability of fragile nanomaterials.

The MgO@meso-SiO<sub>2</sub> catalyst converted 85% of the ethylenecarbonate, and there were no morphology changes in 10 sequential runs, whereas uncoated, flowerlike MgO broke into pieces after merely one run (Figure 8). This approach created a worthwhile route for making highly active, yet fragile nanostructured catalysts practical for scale-up applications [120].

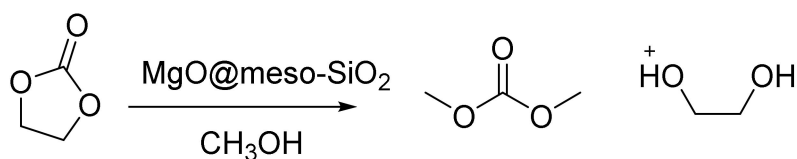


**Figure 8.** Synthesis of DMC on the  $\text{MgO@meso-SiO}_2$  catalyst.

#### 4.2.4. Dehydration

Mesoporous silica usually demonstrates interesting catalytic activity when it comes to dehydration and dehydrogenation reactions. Recently, Fan et al. reported on a series of mesoporous silica materials that were embedded in zirconium and phosphotungstic acid via a sol-gel process [121]. They studied conversions of D(-)-fructose catalyzed by a synthetic mesoporous silica nanocatalyst that produced 5-(hydroxymethyl)-furfural as the main product. They also examined the relationship between the structure and activity of the catalyst as well as its ambient reaction and found that it exhibited good recycling potential (Figure 9). The characterization results revealed that the mixed template copolymer and PVP had flake-like silicates and that both zirconium and phosphotungstic acid were operating as recyclable nanocatalysts capable of good performances. The catalytic process revealed that water was the most appropriate green solvent for the transformation of D(-)-fructose into fine chemicals. Moreover, cholesterol doping in a sol-gel preparation resulted in the formation of more active catalysts. Furthermore, the addition of phosphotungstic acid to the sol-gel had a positive effect on the final yield of the reaction in ethanol.

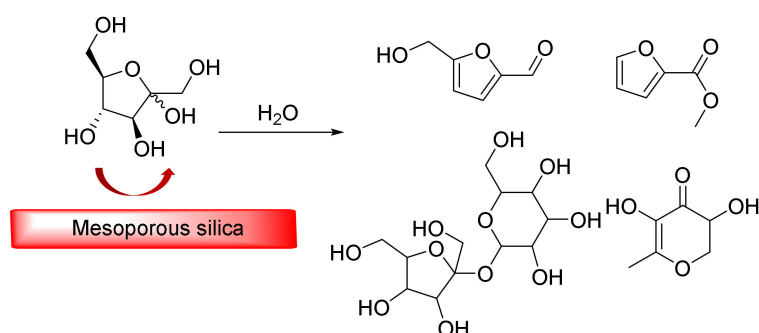


**Figure 9.** The dehydration of D(-)-fructose in the presence of mesoporous catalysts of zirconium and phosphotungstic acid.

In addition, xylose dehydration via a functionalized KIT-6 catalyst was reported by Smart et al. (Figure 10). They showed that the selective and efficient dehydration of xylose to furfural in a water/toluene *bi*-phasic system could be achieved by means of a sulphonic acid-functionalized KIT-6 catalyst. This optimal catalyst provided both high furfural selectivity and xylose conversion (more than 94%). Furthermore, this heterogeneous  $\text{SO}_3\text{H-KIT-6}$  catalyst had high efficiency and could be recycled without further treatment for up to three runs [122].

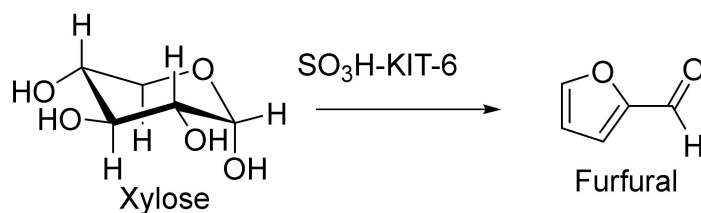


**Figure 10.** Xylose dehydration in the presence of the  $\text{SO}_3\text{H-KIT-6}$  catalyst.

Compared to previously reported catalysts, the heterogeneous SO<sub>3</sub>H-KIT-6 catalyst converted more xylose and also had the highest furfural selectivity under the applied reaction conditions, as shown in Table 1.

**Table 1.** Comparison of the furfural yield obtained using different raw materials and catalysts.

Raw Material	Catalyst	Solvent	Yield (%)
Polysaccharide	HCl	H <sub>2</sub> O/MIBK	33.3
Corn cob	H <sub>2</sub> SO <sub>4</sub>	H <sub>2</sub> O/Toluene	65.5
Wheat straw	CrPO <sub>4</sub>	NaCl/THF	67
Xylose	CrPO <sub>4</sub>	NaCl/THF	88
Biomass	SnXCsyPW	DMSO/H <sub>2</sub> O	63
Hydrolysate	HZSM-5	H <sub>2</sub> O	75
Xylose	SO <sub>3</sub> H-KIT-6	H <sub>2</sub> O/Toluene	92

#### 4.2.5. Condensation

The hybrid mesoporous SBA-15 functionalized with choline hydroxide (Chol-SBA-15), hexamethyldisilazane as a capping agent (Chol-HMDS-SBA-15) and mesoporous silica microspheres (Chol-MSM) was created for the co-condensation method developed by Hierro et al. These Brønsted base solid materials were tested successfully as catalysts in Knoevenagel condensation reactions of benzaldehyde with malononitrile and ethylcyanoacetate (Figure 11). These catalysts were easily recovered, and separation made them reusable, and hence eco-friendly, for several cycles without loss of activity. The Chol-MSM catalysts showed high catalytic activity and 99% selective conversions of ethyl-2-cyano-3-phenyl acrylate. In addition, their reusability without loss of activity has been demonstrated [123].

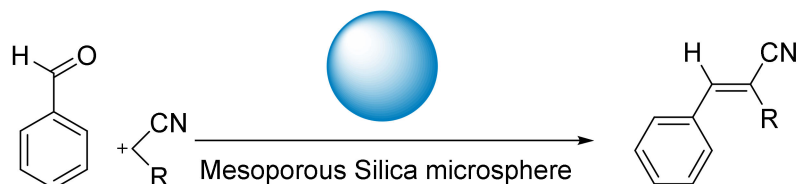


**Figure 11.** Knoevenagel condensation in the presence of a mesoporous nanosilica microsphere.

Additionally, an interesting catalyst of cylindrical Fe-MCM-41-ionic liquid (Fe-MCM-41-IL) was prepared by anchoring an acidic triazolium IL on the surface of Fe-loaded MCM. This cylindrical, mesoporous Fe-MCM-41-IL acted as an efficient, reusable, heterogeneous nanocatalyst for the one-pot synthesis of pyrimidine derivatives, producing high yields under mild conditions (Figure 12). Its operational simplicity, high yields, low cost, eco-friendly reaction conditions, reusability, and recoverability make this procedure much greener than the other reported procedures. Interestingly, this catalyst can be recovered via an external magnetic device [124].

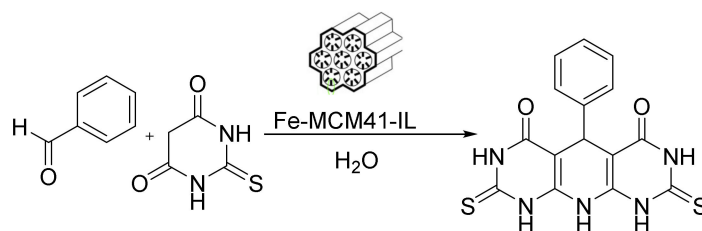


**Figure 12.** Knoevenagel condensation through cylindrical Fe-MCM-41-IL.

#### 4.2.6. Hydration—Asymmetric

The facile synthesis of some multifunctional heterogeneous catalysts through Au/carbene assembly and a chiral Ru/diamine dual complex in mesoporous silica was reported by Xia et al. They also offered a synthetic approach for constructing a multi-functional mesoporous catalyst for an enantioselective tandem reaction. They demonstrated the one-pot enantioselective hydrogenation of a hydration–asymmetric transfer tandem reaction, creating chiral nifenalol with up to 99% enantioselectivity (Figure 13) [118].

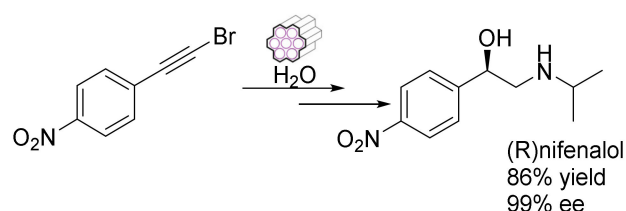


**Figure 13.** Asymmetric-hydration through chiral mesoporous nano silica.

#### 4.2.7. Mukaiyama Aldol Reaction

The heterogeneous catalysts can be highly recyclable catalysts, which is particularly crucial when utilizing valuable metal catalysts. Furthermore, applying metal oxides to diverse supports seems to be a good way of creating, e.g., Lewis acid (LA) catalysts. Xu et al., reported that Fe-SBA-15 and Fe-MCM-41 (Figure 14), different iron-containing mesoporous silicas, could be synthesized through a versatile and straightforward method involving iron acetylacetonate as a metal species. Furthermore, a pH adjustment during the synthesis was found to improve the iron content. The acidity of the surface was tested via a series of Hammett indicators. Using a nonporous catalyst as an LA was monitored in the Mukaiyama aldol reaction. The LA catalytic activities of the materials were particularly fine-tuned, and the corresponding aldol products exhibited good selectivity and yield. The catalysts were stable and reused at least nine times [125].

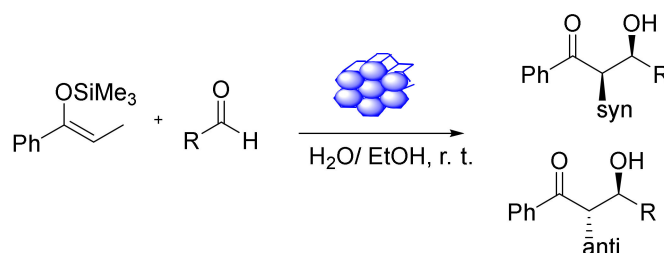


**Figure 14.** Mukaiyama aldol reaction in the presence of Fe-MCM-41-LA.

The XRD (X-ray diffraction) analysis of the iron-modified mesoporous silica showed there were no iron oxide species [125]. Moreover, FT-IR spectroscopy of the iron-modified mesoporous silica revealed a significant majority on the LA site compared to the Bronsted site. The iron species deposited on mesoporous silica can function as highly selective and active sites for the Mukaiyama aldol reaction of various aldehydes with phenyl-1-(trimethylsilyloxy)-propene and trimethylsilyloxycyclohexene. The experimental procedure using a clean solvent system was straightforward, and no harmful organic solvents were used. The catalyst could be recovered and used once again the same reaction without loss in activity. The iron-modified mesoporous silica nanocatalyst is an extremely active heterogeneous LA catalyst and could be applied in many other reactions and numerous environmentally friendly chemical transformations in organic chemistry.

#### 4.2.8. Esterification

Magnetic mesoporous silica with cobalt ferrite ( $\text{CoFe}_2\text{O}_4$ ) nanoparticles embedded in the silica exhibited a strong paramagnetism property and magnetic responsiveness. The esterification catalytic activities of the [BsAIM][OTf]/SCF [1-allyl-3-(butyl-4-sulphonyl) imidazolium] [trifluoromethanesulphonate]/silica cellular foam) (Figure 15) nanoparticles were evaluated via oleic acid with straight-chain alcohols and exhibited decreases in the pore diameters and specific surface area of MPS-SCF (MPS: 3-Mercaptopropyl trimethoxysilane) while increasing the SH loading of MPS-SC (SC: Silica cellular). More SH groups on MPS-SCF and the fewer IL were immobilized on [BsAIM][OTf]/SCF owing to IL's smaller pore diameters, which delayed the immobilization and diffusion of [BsAIM][OTf]. [BsAIM][OTf]/SCF has some applications in shape-selective catalyzes, and this catalyst with different structures has participated in different reactions [126].

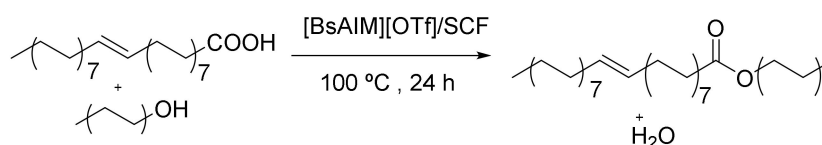
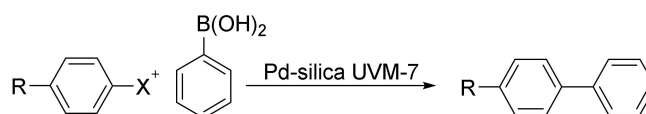


Figure 15. Esterification reaction of oleic acid through [BsAIM][OTf]/SCF.

#### 4.2.9. Suzuki-Miyaura Cross-Coupling Reactions

The Suzuki–Miyaura (S-M) cross-coupling reactions are important in the synthesis of biologically substitutable aromatic compounds. Perez et al., reported a convenient S-M cross-coupling reaction through a new Pd (0) catalyst supported on silica UVM-7 (Scheme 1) [126].



Scheme 1. Suzuki-Miyaura reaction.

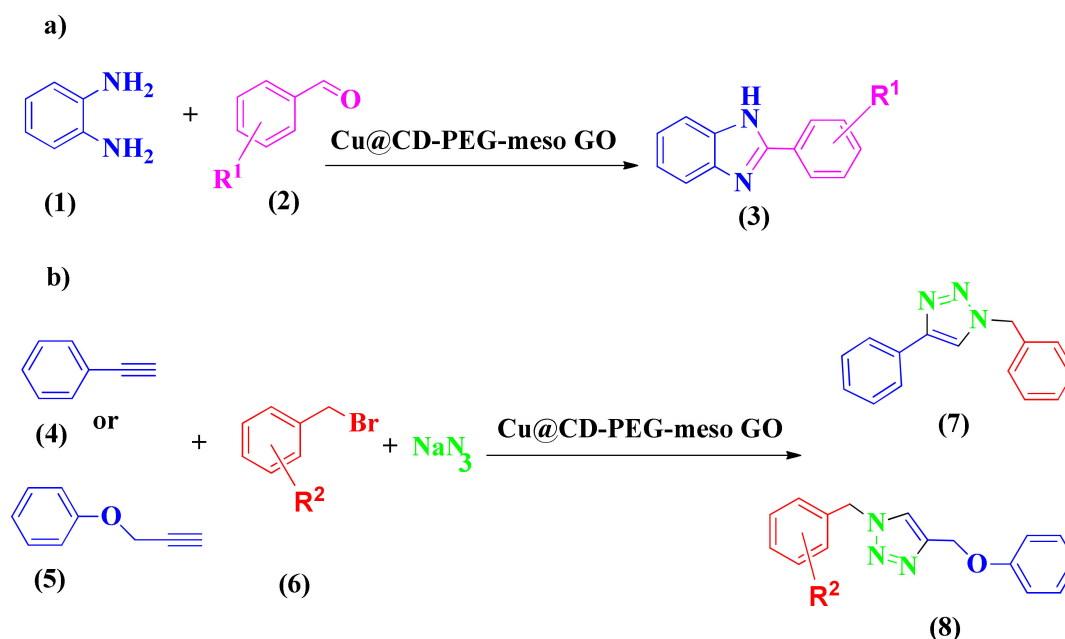
The catalyzed S-M cross-coupling reaction of arylhalide with arylboronic acid is one of the most efficient approaches for the synthesis of biaryls and triaryls as well as the introduction of substituted aryl moieties into organic transformations. The great dispersion, activities, and small sizes of the palladium nanoclusters to be fixed on the silica surface were tested for S-M reactions using different phenylboronic acids with 4-substituted phenyl halides. In their study, facile S-M cross coupling was carried out by Pd species originating in the partial solubilization of Pd immobilized on mesoporous silica.

#### 4.2.10. Cycloaddition Reaction

One of the most efficient synthetic tools for the convenient preparation of triazole derivatives in a regioselective manner is the click reaction [127]. Azole scaffolds are utilized in many biological applications, including the treatment of tumors [128,129], allergies [130], HIV [131], and microbial diseases [132–137]. Copper species catalysts are some of the most important catalysts in modern organic transformations [138,139].

Khalili et al. reported cyclization reactions through a copper-based catalyst, i.e.,  $\text{Cu}@\beta\text{CD}$  ( $\beta$ -cyclodextrin) PEG-meso-GO NPs [140]. The hydrophilic and waterproof characteristics of NPs are provided by PEG. In addition,  $\beta$ -CD can be used as an efficient ligand for the Cu catalyst and help the phase transfer into the aqueous phase [141–144]. Copper species play critical roles in the cycloaddition reaction needed to synthesize 1,2,3-triazole and the click and oxidation reactions necessary for synthesizing benzimidazole derivatives (Scheme 2a,b, respectively). The activity and efficiency of  $\text{Cu}@\beta\text{CD}$ -PEG-meso-GO NPs as a catalyst was estimated for the click reaction and C-N bond oxidation. It was shown to be a water tolerance, efficient, and recyclable catalyst [145–148].

The benefits of these green procedures (water was used as a solvent) were their high-yield reactions at short reaction times without laborious purification, plus the catalyst was easily recoverable and water dispersible. These NPs exhibited good reusability without significant decreases in activity.



**Scheme 2.** Syntheses of benzothiazole (a) and 1,2,3-triazole (b) via Cu@βCD-PEG-meso-GO.

Additionally, the tetrazole scaffold is one of the most important heterocycles and has wide-ranging applications in hormonal, antibacterial, and anti-inflammatory areas [149,150]. A one-pot, three-component green synthesis of tetrazole cycloadducts was carried out through a Cu-Fe<sub>3</sub>O<sub>4</sub>@SiO<sub>2</sub>-PVA NP catalyst by Sardarian et al. [151]. The heterogeneous magnetic performance of this NP was studied in the N-arylation of amines with aryl halides in high-yield syntheses of 1H-tetrazoles without external ligands. The advantages of this green procedure were the low amount of catalyst used, ease of separation, good reusability, and excellent yields of the final products [151].

#### 4.2.11. Ullman Coupling

The Heck, Suzuki-Miyaura, Sonogashira, and Ullmann reactions have been shown to be excellent methods for generating carbon-carbon bonds through catalyzed cross-coupling reactions [152–155]. Aryl-aryl bond formation reactions are amongst the versatile strategies involved in the synthesis a wide range of products, including agrochemicals, pharmaceuticals, natural products, and conducting polymers [156–158]. Yavari et al. reported that Pd-poly(N-vinyl-2-pyrrolidone)/MCM-48 NP is an efficient, heterogeneous, recyclable catalyst for the Ullmann cross-coupling reaction. This environmentally friendly catalyst exhibited high catalytic activity, easy separation, and reusability [159]. This reaction was carried out in a DMF medium at 100 °C and produced good yields. The activation of the C–Cl bond proved to be more difficult than the activations of the other alkyl-halide bonds, and it mostly requires harsher conditions in heterogeneous catalytic systems.

### 5. Application of Silica Mesopores in Drug Delivery

In recent decades, significant advancements in pharmaceutical industry and medicinal chemistry have led to deep understanding of physico-chemical properties of medical compounds and provided the opportunity for recognition of cellular absorption strategies for effective treatments [160–164]. Initially, in some cases, such as chemotherapy for cancer, therapeutic methods relied on the use of toxic drugs with undesirable complications and limited beneficial effects [165]. To overcome this problem,

targeted drug delivery carriers (TDDCs) were designed to deliver effective doses of drugs to targeted tissue cells [166]. The success of these drugs depends on the fabrication of bioavailability carriers with high drug loading capabilities and no early release [165]. The drug delivery agent should have a compatibility with the drug [166], be capable of encapsulation [167], feature high drug loading [168], and have the appropriate release rate [169]. Due to their importance, changeless drug delivery systems are focused structurally so that drug materials are transmitted without immediate release to the target site [165]. Among the many sustained carriers, mesoporous silica materials with a specific surface structure are capable of gradually releasing various drugs and controlling this process [170]. Mesoporous silica materials are attractive due to their resistance to heat [171], pH [172], resistance to mechanical stress [173], very small pore sizes [174], and have more potential compared with other *Nano*-carriers in terms of greater accuracy in the selective loading of various drug molecules and their large pore volumes available for drug loading [175]. The use of a silica mesostructure for the purpose of drug delivery was reported in early 1983. Since that time, silica nanoparticles have been used widely as drug carriers due to their high biocompatibility and easy formulation with medicines. A wide range of drugs is used, such as small molecules, photosensitized molecules, proteins, deoxyribonucleic acids, and ribonucleic acids with silica carriers, in the treatment of diseases such as cancer, Parkinson's disease, and heart problems. The use of silica nanoparticles to deliver bioactive molecules could protect these molecules from degradation while allowing controlled release, prolonged circulation in the blood, improved disease targeting, and reduced side effects [176].

In this section, drug deliveries induced by endogenous and exogenous stimuli, including pH, redox, enzymatic, glucose, H<sub>2</sub>O<sub>2</sub>, adenosine triphosphate (ATP), temperature, light, magnetic field, and ultrasound stimuli, will be discussed.

### 5.1. pH-Responsive Drug Delivery

Since the pH readings in tumors or inflammatory sites (pH ~ 6.8), as well as endosomal or lysosomal compartments of cells (pH ~ 5–6), reveal acidic conditions, a number of nanocarriers, such as mesoporous silica nanoparticles (hereafter as MSNs), have been exploited for controlled drug delivery. Casaus et al., studied an ionically controlled nanoscopic molecular gate that was developed by exploiting functionalized mesoporous materials [176]. This study showed that control of mass transport at a nanometric scale can be achieved by using rigid solids and molecules that are active at physiological, pH-active molecules. In another study, Kawi et al. examined the performance of amin-functionalized mesoporous silica SBA-15 loaded with bovine serum albumin (BSA) encapsulated within a polyacrylic acid (PAA). The entrapped BSA was released from the PAA-encapsulated silica SBA-15 at a pH of 7.4 rather than at a lower pH value of 1.2 [177]. They found that this material has the potential for releasing protein drugs to sites with higher pH values, such as the small intestine or colon. Hong et al. studied covalently immobilized PAA on MSN materials as a pH-sensitive drug delivery system. In this study, reversible addition-fragmentation chain transfer (RAFT) functionalities were attached to the exterior surface of the MSNs (Figure 16). Their results showed that the PAA-coated MSN could control the access of guest molecules by adjusting the pH value [178]. In 2013, Meng et al. examined an MSN-based, pH-responsive drug release system with polyelectrolyte multilayers. The results showed that MSN under the acidic condition (pH ~ 5.2) had a higher drug release rate than it did under the neutral condition (pH ~ 7.4). Hong et al. used cyclodextrin as a blocking agent for mesoporous channels and *N*-methylbenzimidazole (MBI) as a holder [178]. The channels were designed so that cyclodextrin formed a stable complex at a pH of 7.4 through interactions with MBI. However, in the acidic environment of the cancer cells, the cyclodextrin is released by the MBI. Zinc et al. developed mesoporous materials that due to pH = 0 values, could not release propidium iodide (PI) [179]. However, the drug could be released when the pH was low or high. In their work, cucurbit (CB) [180] and uril [180] were used as holders. Xiao et al. synthesized pH-responsive mesoporous materials, wherein polycation poly(dimethylethyldi-allylammonium chloride) (PDDA) interacted with anionic mesoporous material-based carboxylic acid at a pH = 0 [181]. In this case, the channel was closed,



and the vancomycin drug was trapped within the mesoporous materials. The carboxylic acid was protonated in the acidic condition, eliminating the interactions between polycation and carboxylic acid; thus, polycation was removed from the surface, and the drug was released. Gisbert et al. synthesized a type of pH-responsive gate keeper MSNs with self-immolative polymers blocking and the pore opening, which triggered drug release by acidic pH. The pH sensitivity of this nanosystem causes that cargo release took place in acidic conditions, while there was almost no release at physiological pH [182]. In such systems, controlled drug release at special time and space, on demand, could be achieved with a zero-release effect in blood circulation to prevent drug decomposition. Several controlled drug delivery nanovesicles based on organic and inorganic platforms have been fabricated [183–185]. Xingmei et al. prepared a tumor-adhesive pH-degradable PVA microgels decorated with tissue-adhesive dopamine moieties by a combination of microfluidics technology and photo-cross-linking chemistry with a considerable conceptualization efficiency of bevacizumab (Bev) and docetaxel (DTX) to enhance breast cancer chemotherapy. The results showed that MSN under the acidic condition (pH ~ 6.5) had an acceptable drug release rate e.g., ca. 73% [186].

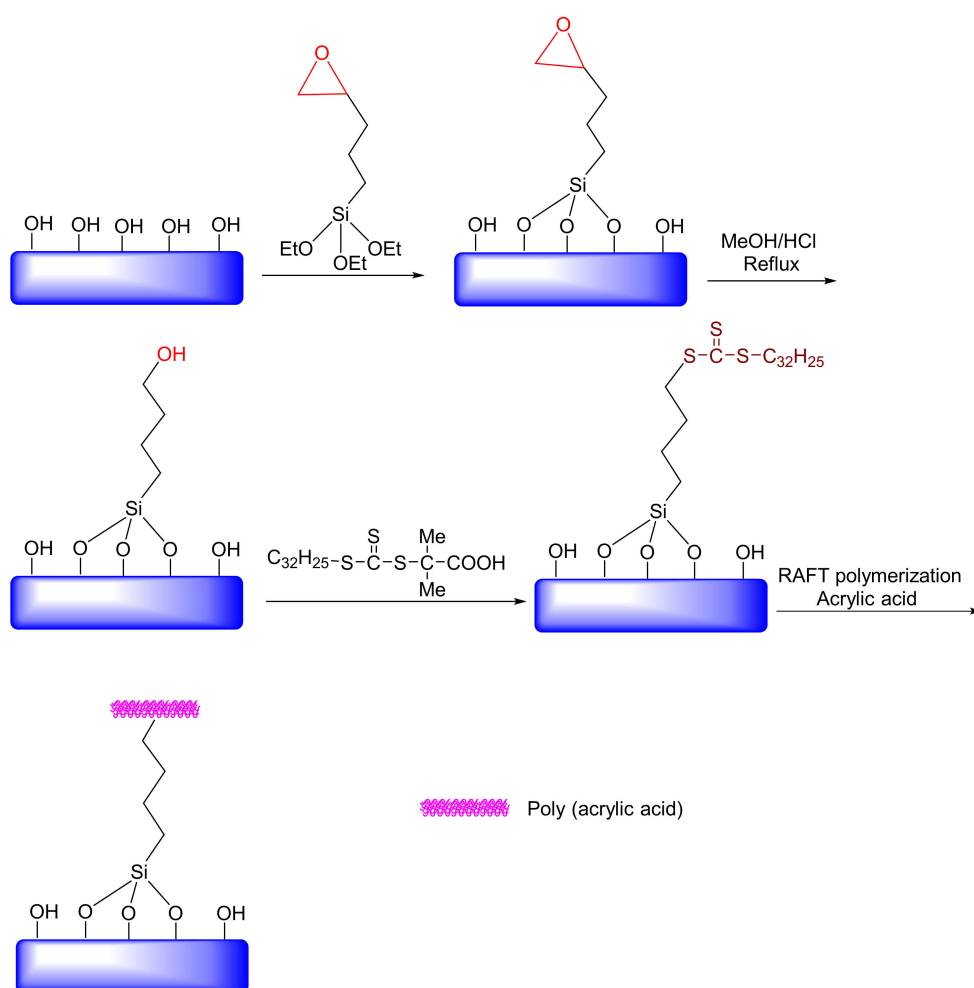


**Figure 16.** Forming reversible addition-fragmentation chain transfer (RAFT) agent-coated mesoporous silica nanoparticles (MSNs) as the novel, smart nanocontainers incorporating an MSN for pH sensitivity.

## 5.2. Redox-Responsive Drug Delivery

Many studies have been conducted about redox-responsive delivery systems with disulphide bonds, which extensively can be applied to attach to different gatekeeper such as peptides [187], antibodies [188], and proteins [189]. During the reduction of glutathione into sulfhydryl groups, the disulphide bonds break readily, which destroys the carriers and facilitates the release of the cargo.

Zhong et al. performed an experiment on attachment of collagen to MSNs by a disulphide linker followed by introduction of lactobionic acid, which resulted in redox-responsive system for cell-specific intracellular drug delivery and efficient endocytosis [189]. Other studies have investigated diselenide bonds, which have reduction sensitivities and redox-responsive abilities that are similar to those for disulphide bonds. In tumor therapy, more sensitive redox-responsive delivery systems can be designed with diselenide bonds due to the lower energy of Se-Se bonds compared to S-S bonds and C-Se bonds (Se-Se 172, C-Se 244, and S-S 268 kJ/mol). In addition to disulphide and diselenide bonds, there are some studies that have examined the succinimide-thioether linkage, delivery systems with trimethyl-locked benzoquinone (TMBQ), and some other delivery systems [190]. In another study, Lin et al. investigated the role of the S-S bond in drug release [187]. First, they synthesized a mercapto acetic acid covered with CdS nanocrystals. CdS, due to its small size, can penetrate meso-channels conventionally, thus blocking them and preventing the drug's exit. Therefore, CdS is dissociated by reducing agents and released from inside the cavity; subsequently, the drug is released from the nanopores (Figure 17).

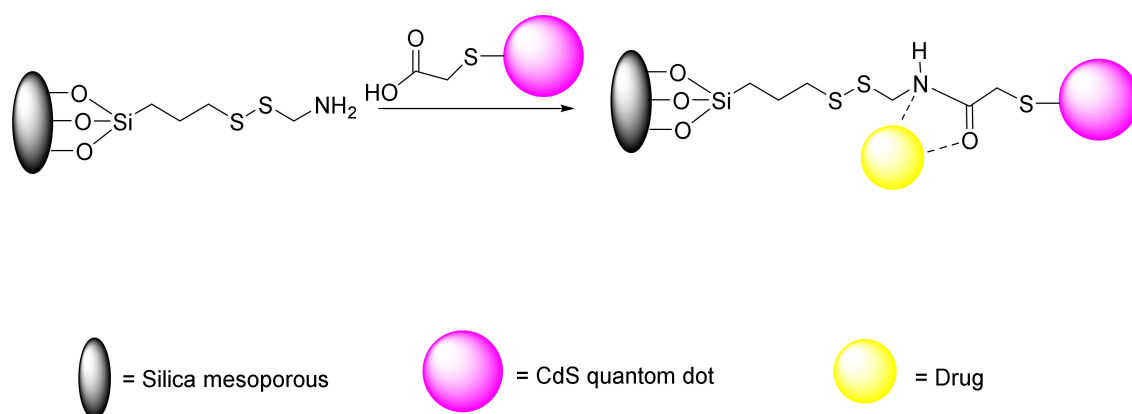


**Figure 17.** CdS/MSN-mercapto acetic acid as a nanocarrier for drug delivery system (DDS).

### 5.3. Enzyme-Responsive Drug Delivery

Due to their biocompatibilities and specific biological activities, enzymes are suitable for the design of controlled-release delivery systems [190]. Liu et al. designed a biocompatible matrix metalloproteinase (MMP)-responsive drug delivery system based on MSN (Figure 18) [191]. In this study, they used BSA as an end-capping agent, a functional polypeptide as an intermediate linker, and lactic acid (LA) as a targeting motif for releasing doxorubicin (DOX) in vivo. The in vivo experiments have shown that the system can inhibit tumor growth efficiently with minimal side effects. Other studies have investigated on the multifunctional stimulus-responsive nano vehicles that were constructed via peptide mediated core/satellite/shell assembly for targeted protease imaging and controlled drug release [192,193]. Zheng et al. used gold nanoclusters based on MSNs through the conjugation of peptide cathepsin B to form MSNs@GNC with a core/satellite structure. The peptide-mediated core/satellite/shell nanocomplexes could be utilized as multifunctional nanovehicles for precise and dynamic imaging of cathepsin B and of controlled drug release [193].

Ren et al. used hyaluronic acid (HA) to modify silica mesopores in a smart drug delivery response to the enzyme hyaluronidase (HD) [194]. HA, in addition to blocking mesoporous channels, can also operate as a target ligand. This modified nano-carrier has interesting features, including a simple chemical structure, high colloidal stability, good biocompatibility, good cell targeting, and good drug release control. HA decomposes when it reaches the infected cell due to excessive congestion with the HD enzyme, and the drug is released. The rhodamine model was utilized in this study. They confirmed the release rates of the drug in the presence and absence of the HD enzyme to ensure the system's responsiveness to the enzyme. The amount of drug released in the proximity of the HD enzyme was much greater than the amount of the drug released without the enzyme in an acetate buffer

(pH = 4.5) and a PBS buffer (pH = 7.4). Bernardos et al. used lactose to fill mesoporous cavities [195]. Galactose has a large structure and, through this structure, prevents the release of pyridine ruthenium ( $[\text{Ru}(\text{bipy})_3]^{2+}$ ) in a drug model. When lactose is in contact with the galactosidase enzyme, it is hydrolyzed into galactose monosaccharide and glucose, and the resulting small structure causes the drug to escape from the cavities. Kleitz et al. choose an enzyme-sensitive system that was able to reduce the azo linkage [196]. Mesoporous was converted to mesoporous with an iodine functional group; at a later stage, sulphasalazine was coupled to it, and two sulphapyridine and 5-amino-salicylic acid drug precursors were loaded. Due to the placement of the mesoporous in the surrounding enzyme reductase, the azo bond was broken, and the drug was released. Zinc et al. studied drug delivery to liver tissue using mesopores [197,198]. Silica mesopores were modified via an intracellular cyclodextrin complex. The addition of the cyclodextrin and the loading of rhodamine as a drug material were accomplished simultaneously. To prevent a click reaction from taking place, a bulking group was attached to cyclodextrin, which connected to the mesopores with two esters and amid linkers. These two bonds are desirable when evaluating the effect of liver enzymes. However, the key factor is which linkage is hydrolyzed under these conditions. The results indicate that the ester bond was rapidly hydrolyzed. As a result, the bulk group was exited, and the drug was released.

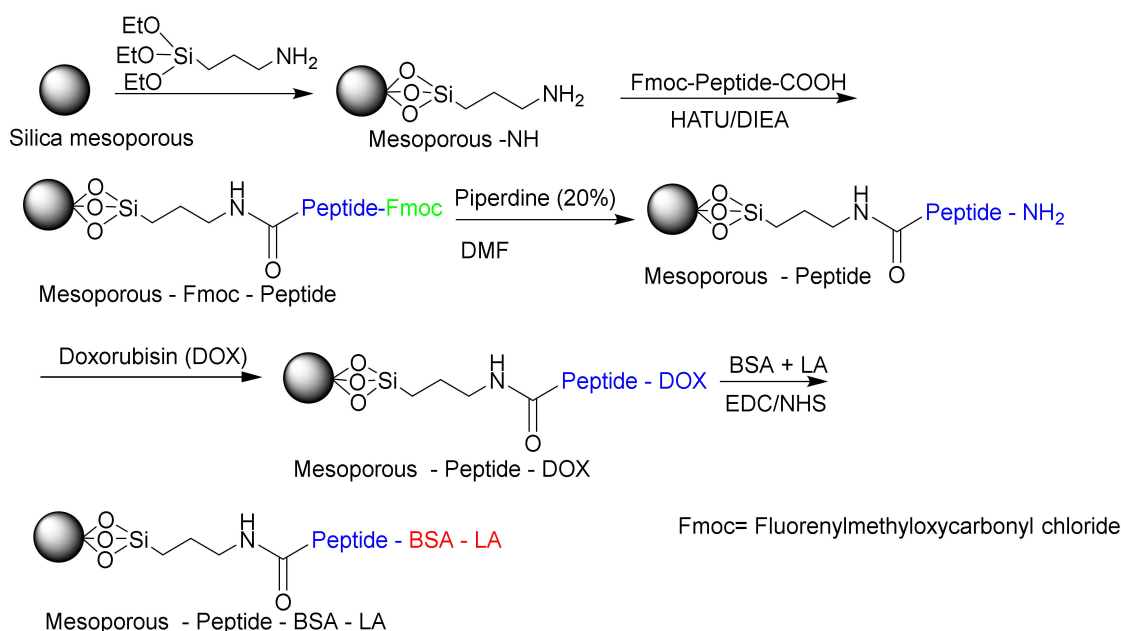


**Figure 18.** Matrix metalloproteinases (MMPs) based on MSNs (mesoporous-peptide-BSA-LA) responsible for releasing DOX in vivo.

#### 5.4. Glucose-Responsive Drug Delivery

Zhao et al. synthesized a nano-carrier mesoporous silica nanoparticle-based drug delivery system for glucose-responsive controlled release [199]. The glucose-responsive controlled release consisted of insulin and cyclic adenosine monophosphate (cAMP). Gluconic acid-modified insulin (G-Ins) was attached to the surface of the mesoporous MSN carrier, and cAMP molecules were encapsulated inside the MSN. This system is suitable for the treatment of diabetes because it responds to just the glucose levels in the blood. In addition, the cyclic adenosine cAMP, known as an insulin secretion stimulating agent, can be encapsulated inside the pores, and then released subsequent to G-Ins diffusion to regulate blood glucose levels (Figure 19). Aznar et al. have described the use of glucose oxides conjugated with cyclodextrin as pore blockers of MSNs, which was previously functionalized with propyl benzimidazole groups in order to form an inclusion complex with the cyclodextrin [200]. When glucose is added, glucose oxide decomposed this molecule into gluconic acid and resulted in a pH drop which induces the protonation of the benzimidazole, opening the pore. Hei et al. designed an

insulin delivery based on MSNs, which showed positive correlation with the species and concentration of saccharides [201]. They proposed that the designed insulin delivery system presented glucose responsiveness even in the serum but also a good biocompatibility toward liver cells.

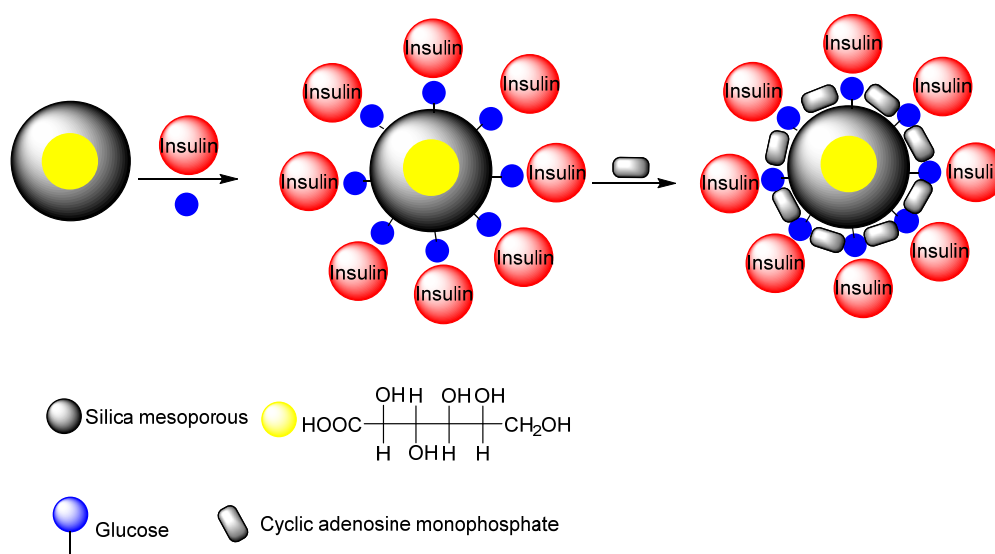


**Figure 19.** The insulin secretion stimulating agent cAMP is encapsulated inside MSN and used for DDS release subsequent to G-Ins diffusion to regulate blood glucose levels.

### 5.5. $H_2O_2$ -Responsive Drug Delivery

Targeting  $H_2O_2$  as a diagnostic marker and therapeutic agent has shown great potential. In 2012, Geng et al. reported on a biocompatible delivery platform based on an  $H_2O_2$  responsive, controlled-release system using mesoporous silica nanoparticles to realize the targeted delivery of the therapeutic metal chelator for treating Alzheimer's disease [202]. Increasing the levels of  $H_2O_2$  led to the release of the metal chelator. The advantages of this delivery system are its excellent biocompatibility, good cellular uptake, and appropriate intracellular release of metal chelators. Hence, this delivery system shows the potential for controlled drug release applications. Guo et al. reported a temperature and  $H_2O_2$  dual-responsive nanovalve, which were fabricated from ferrocene modified MSNs and cyclodextrin-poly(N-isopropylacrylamide) star shaped polymer due to the host-guest interactions for controlled drug release and exhibited excellent anti-cancer activity [203].

### 5.6. ATP-Responsive Drug Delivery

ATP is the most abundant ribonucleotide used in cells as a co-enzyme, and it can be used as a trigger for the controlled release of anticancer drugs. In 2011, Zhu et al. designed a novel and generally bioresponsive controlled-release MSN system based on aptamer-targeted interactions [204]. In their system, the pores of the MSNs were capped by Au nanoparticles that had been modified with the ATP aptamer. They showed that the cargo was released when the MSNs were uncapped in the presence of ATP molecules.

### 5.7. Thermo-Responsive Drug Delivery

As the literature has showed, the local temperatures of tumor sites are generally higher than the temperatures at non-tumor sites. Hence, designing a temperature-responsive drug carrier that only releases drugs at a temperature above  $37^\circ\text{C}$  is a very useful method for killing tumor cells [194,205–207]. Poly(N-isopropylacrylamide) (PNIPAM) is one of the most popular temperature-sensitive polymers. PNIPAM has a low critical solution temperature (LCST). Lopez et al. proposed a method centered on small-sized MSNs that has become widely used due to the ability of the MSNs to control

thermo-responsive drug delivery very well [196]. In this method, PNIPAM was grown on the external surfaces of pre-synthesized MSNs. They showed that the PNIPAM-coated MSNs had no acute cytotoxicity while exhibiting good endocytosis efficiency on human breast carcinoma cells. Zhang et al. synthesized a new nano-carrier based on mesoporous SBA-15 containing  $\text{Fe}_3\text{O}_4$  nanoparticles and PNIPAM temperature-sensitive polymers inside the channels [199]. They increased the concentration of  $\text{FeCl}_2$  in the solution after the formation of the micelles and added TEOS to the system to form a stock sol. During the subsequent condensation reactions in the sol-gel process, surfactants were added to serve as structure-determining agents. Finally, PNIPAM was linked in the mesoporous channels. Yang et al. prepared  $\text{Fe}_3\text{O}_4$  NPs and a mesoporous material, then placed the  $\text{Fe}_3\text{O}_4$  NPs in the center of the material [200]. Only the removal of the CTAB was required for the production of the simple magnetic mesoporous material used, while the temperature-sensitive mesoporous with 3-(trimetoxyl) propylmethacrylate (MPS) was acrylated in order to synthesize the mesoporous. Subsequently, PNIPAM polymerization was observed around the mesoporous material, generating the core-shell mesoporous structure.

### 5.8. Light-Responsive Drug Delivery

Light irradiation is a convenient, remote-control method used in drug delivery systems. Light-sensitive molecules, such as azobenzene (AB), 0-nitrobenzyl ester, and thymine bases, are anchored to the surface of MSNs to render them photochemically susceptible to the light-controlled release [208,209]. Mal et al. described a UV light-induced, reversible-release drug system [206]. They showed that the uptake, storage, and release of organic molecules in MCM-41 can be carried out through the photo-controlled, reversible intermolecular dimerization of coumarin derivatives attached to the surfaces of the pores. In 2009, Park et al. showed that cyclodextrin-covered mesoporous silica nanoparticles with photo-cleavable linkers exhibit photo-induced release characteristics [210]. Lu et al. reported in vivo insertion of AB into the pores [204]. The drugs that were loaded included RB, polyimide (PI), and comptothecin. After the mesoporous silica carrier attacked the target tissue with light irradiation, the azo bond converted rapidly to its trans and cis isomers. Meanwhile, the drug was released from the cavities due to the repulsive force created by the very high mobility of the bulky phenyl-functional groups attached to the nitrogen. Zhao et al. proposed the use of the properties of a complex containing cyclodextrin, namely, its ability to create isomeric cis-and trans-azo, to alter an in vivo delivery time via light [205]. As shown in Figure 20, aromatic compounds were initially substituted for the MSN material. The bulk of the naphthalene then acts as an obstacle to the withdrawal of cyclodextrin. Furthermore, when the azo-isomeric bond is used, cyclodextrin acted as a washer and prevented the release of the drug. After a nanocarrier injection, light irradiation converted the cis-isomer into a trans-isomer, allowing the drug to reach the target site. Tanaka et al. reported on a light-controlled drug delivery system for direct drug release that was based on coumarin cavity sizes [206]. When coumarin is exposed to UV light at wavelengths above 310 nm, it assumes a dimmer structure but returns to monomer form at a shorter wavelength (254 nm). The dimmer of coumarin, which is placed on the surface of the MCM-41 mesoporous material, reduces the size of the effective cavity and prevents the release of drugs loaded inside the channels. Hence, radiation with shorter wavelengths can open the channels and release the drug successfully. One of the main limitations of these devices is the low penetration capacity of UV-Vis light in living tissues. In order to overcome this problem, DDSs capable of responding to NIR radiation, which exhibits higher penetration capacity, have been reported. Au nanoparticles present plasmonic properties that allow them to transform NIR radiation into thermal energy. Chang et al. have reported a system based on Au nanorods encapsulated within MSNs decorated with DNA double stands at gatekeepers [211]. Moreover, Yang and coworkers designed a light-responsive, singlet-oxygen-triggered on demand drug release from photosensitized chlorin e6 doped MSNs nanorods, coated with bovine serum albumin modified with polyethylene glycol for cancer combination therapy [212].

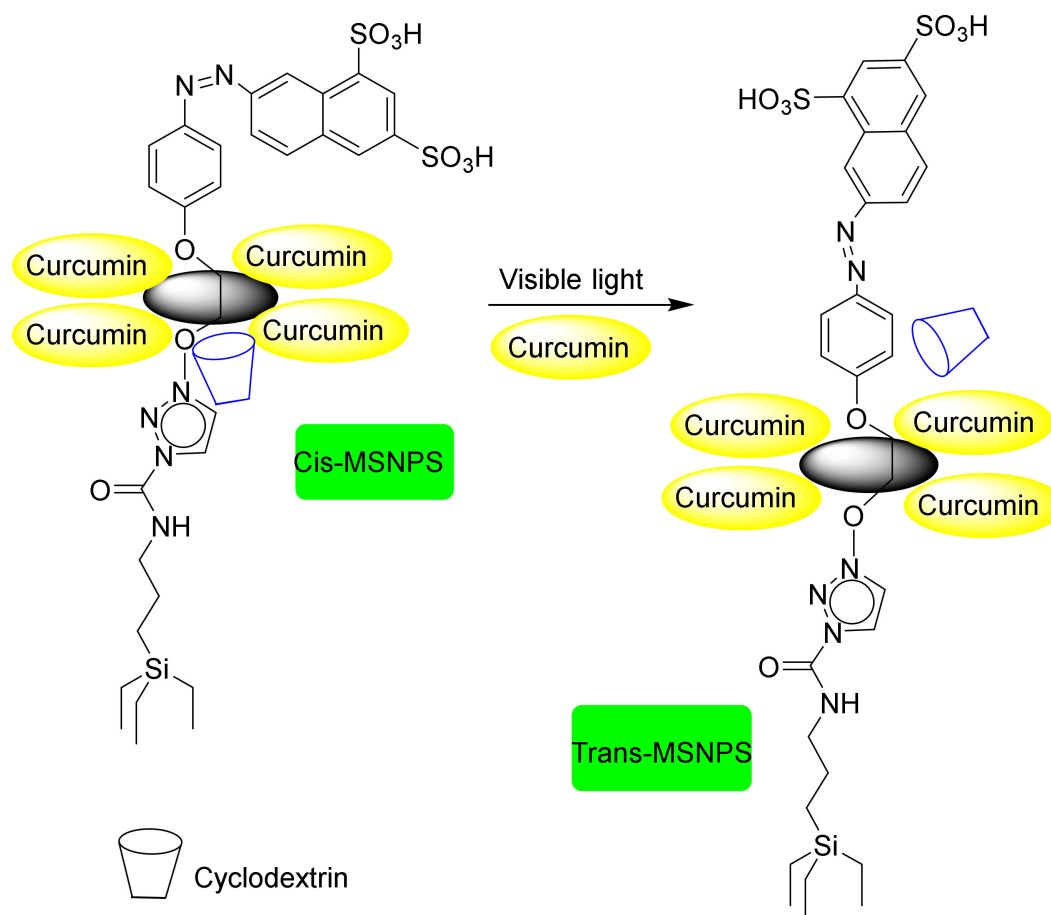


**Figure 20.** Cyclodextrin functionalized with silica mesopores for light-responsive drug delivery.

### 5.9. Magnetic-Responsive Drug Delivery

A magnetic-responsive controlled released system based on magnetic nanoparticles brings drug-loaded nanoparticles to the tumor site under the influence of an external magnetic field. In 2011, Chen et al. constructed  $\text{MSN@Fe}_3\text{O}_4$  by capping MSN with monodispersed  $\text{Fe}_3\text{O}_4$  nanoparticles through chemical amidation [207]. The results of this study showed that in the presence of a magnetic field, the amount of the drug released from the  $\text{MSN@Fe}_3\text{O}_4$  increased. Magnetic-responsive drug delivery is usually dependent on the temperature and nanoparticles, obeying two mechanisms. The first mechanism is the Brownian motion provoked by the fast rotation of the magnetic nuclei, and the second mechanism concerns the Néel functions describing the rotation of the magnetic moments [213,214]. In an interesting report, Yang et al. used an alternating magnetic field (AMF) to heat  $\text{Fe}_3\text{O}_4$  NPs loaded inside the pores [210]. In this work, MSNs were functionalized with the hexadecylmethylenediamine (HDMD) ligand and formulated as a complex. At the time of reinforcement, the drug was also inserted into the mesoporous cavities. Finally, the silica mesopores were exposed to the magnetic field, and, following Hall's law, the  $\text{Fe}_3\text{O}_4$  NP vibrated and released the drug (Figure 21).

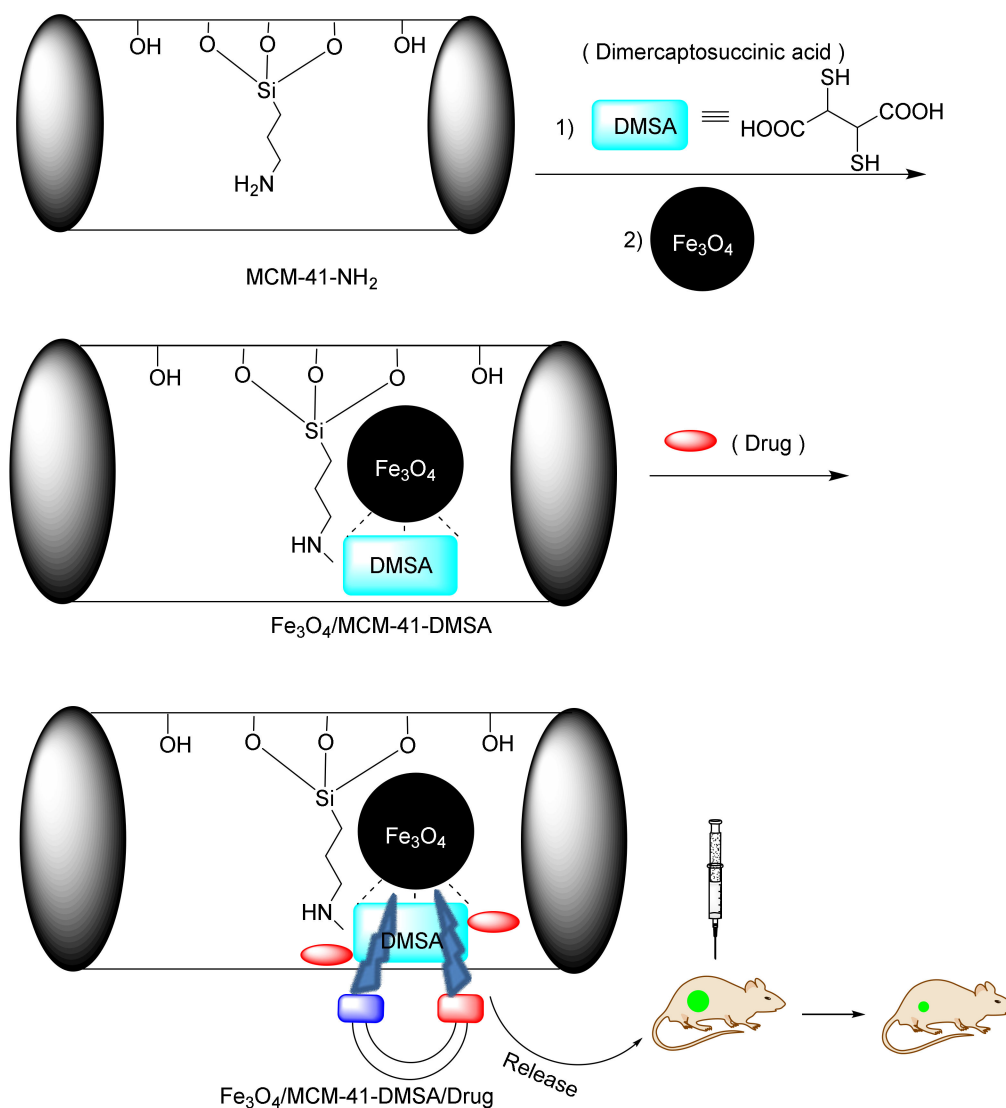


Figure 21.  $\text{Fe}_3\text{O}_4/\text{MCM-41-DMSA}$  used in magnetic-responsive drug delivery.

### 5.10. Ultrasound-Responsive Drug Delivery

Ultrasound-responsive drug delivery belongs to the non-invasive stimulus category. Some studies have shown that ultrasound can induce chemical reactions, even to the point of being able to cleave some chemical bonds. Paris et al., prepared an ultrasound-responsive system on a MSN surface that acted as a pore gatekeeper [215]. In this system, nanoparticles can be loaded with the drug at low temperatures. Their study showed that MSN could be released by remote stimuli, which is essential in drug delivery and cancer therapy.

## 6. Conclusions

Mesoporous-based nanoparticles are a new class of engineered materials that have shown excellent potential for various applications, including as catalysts for the adsorption of pollutants and synthesis of organic compounds, and as drug nano-carriers. In this review articles, some recent advances in the synthesis and some application of well-established and well-studied classes of different mesoporous silica structures, including MCM-41, SBA-15, and SBA-16 are highlighted. We explained that the nanocatalyst-based mesoporous silicas have the ability to remove organic pollutants and can act as an efficient catalyst for the synthesizing the final products with high yields due to the ease with which their surfaces can be modified with various ligands, thus creating appropriate interactions with target

molecules. In drug delivery processes, mesoporous materials have been used as nano-carriers due their adjustable cavities and easy surface functionalization with target molecules and ligands. Due to these properties, drug releases can be accomplished at a target site at a rapid rate through interactions with various functional groups.

In addition, we discuss the parameters that are essential for their syntheses as well as their important applications. When synthesizing mesoporous silica, some factors, such as the type of surfactant material, co-surfactant used, silica source, temperature, alcohol, and pH, influence their morphologies. In this regard, the use of mesoporous silica materials in potential applications requires their modification with different functional groups and affinity ligands. For instance, silica nanoparticles have many silanol groups at their surface that can be exploited for functionalization with various ligands, including drug molecules. Furthermore, these conversions can be controlled via their hydrophilic and/or hydrophobic properties as well as their bonding to guest molecules. Having a network of pores with a highly ordered, homogenously uniform distribution of cavity sizes, high surface areas, large volumes of pores, and easy functionalization makes them suitable for adsorbing hazardous pollutants, organic syntheses, and drug delivery. The observed physio-chemical properties, as well as their diverse applications, show that they have a bright future. In addition, the high versatility of these smart nanosystems opens up opportunities for the development of nanocatalysts and novel nanomedicines for the personalized therapy and diagnosis of many diseases with bad prognosis such as cancer. Finally, the present review article aims to give a brief overview and update on the drug delivery and catalytic applications of the silica mesostructures. By gathering all the research available on this particular topic and writing up a wide and deep review, this study will serve as a reference for chemists in both industry and academia sectors.

**Author Contributions:** M.M.: Main idea, supervision, final writing the manuscript. K.S.: First-draft preparation. M.B.Z.: Data analysis and collection, software. M.D.: First-draft preparation. S.T.K.: Data analysis and collection, software. J.S.: Data analysis and collection, software. A.F.: First-draft preparation. H.M.: Co-supervision, final writing the manuscript. All authors have read and agreed to the published version of the manuscript.

**Funding:** This research was funded by Ferdowsi University of Mashhad, and “The APC was funded by Ferdowsi University of Mashhad”.

**Acknowledgments:** M.M. gratefully acknowledges the financial support from the Ferdowsi University of Mashhad, the Iran Science Elites Federation (ISEF), Zeolite and Porous Materials Committee of Iranian Chemical Society and the Iran National Science Foundation (INSF). M.M. also acknowledges the Cambridge Crystallographic Data Centre (CCDC) for access to the Cambridge Structural Database. H.M. acknowledge the association of the Chemical Industry, the Chemical Industry Fund for the financial supports.

**Conflicts of Interest:** The authors declare no conflict of interest.

## Abbreviations

DDS	Drug delivery system
SBA	Santa Barbara amorphous
MCM	Mobile crystalline matter
FSM	Folding shield mechanism
TUD	Delft University of Technology
HMS	Hollow mesoporous silica
LCT	Liquid crystal templating
CTAB	Cetyl trimethylammonium bromide
HDTMA	Hexadecyltrimethylammonium
PS-b-PAA	Polystyrene-b-poly (acrylic acid)
TEOS	Tetraethyl <i>ortho</i> -silicate
GSs	Gemini surfactants
NTA	<i>N</i> - tributylamine acetate
SDS	Sodium decylsulphate
TMOS	Tetramethyl <i>ortho</i> -silicate
TPOS	Tetrapropyl <i>ortho</i> -silicate



TMS	Trimethoxysilane
TBOS	Tetrabutoxysilane
CMT	Critical micelle of the temperature
CP	Cloud point
EO	Ethoxy
CPP	Critical packing parameter
EG	Ethyleneglycol
RS	Sudan red
MB	Methylen blue
MPS	3-Mercaptopropyl trimethoxysilane
S-M	Suzuki-Miyaura
TDDCs	Targeted drug delivery carriers
ATP	Adenosine triphosphate
BSA	Bovine serum albumin
PAA	Polyacrylic acid
RAFT	Reversible addition-fragmentation chain transfer
HDMD	hexadecylmethylenediamine
PI	Propidium iodide
PDDA	Poly (dimethylethyldi-allylammonium chloride)
MMPs	Matrix metalloproteinase
DOX	Doxorubicin
MO	Methyl orange
MR	Methyl red
MG	Malachite green
EB	Everazol blue
4-NP	4-nitrophenol
RhB	Rhodamine B
PDA	Polydopamine
DBT	Dibenzothiophene
DMDBT	Dimethyldibenzothiophene
BT	Benzothiophene
DT	Dithiophene
THPC	Tetrakis (hydroxymethyl) phosphonium chloride
MNPs	Magnetic nanoparticles
MMNP	Magnetic mesoporous nanoparticle
$\epsilon$ -CL	$\epsilon$ -caprolactone
DMC	Dimethylcarbonate
HMDS	Hexamethyldisilazane
MSM	Mesoporous silica microspheres
LA	Lewis acid
XRD	X-ray diffraction
cAMP	Adenosine monophosphate
G-Ins	Gluconic acid-modified insulin
PNIPAM	Poly(N-isopropylacrylamide)
LCST	Lower critical solution temperature
[BsAIm][OTf]/SCF	[1-allyl-3-(butyl-4-sulphonyl) imidazolium] [trifluoromethane-sulphonate]/silica cellular foam
SC	Silica cellular
$\beta$ -CD	$\beta$ -cyclodextrin
MPS	3-(trimetoxyl) propylmethacrylate
AB	Azobenzene
PI	Polyimide

AMF	Alternating magnetic field
HD	Hylanuridase
MBI	N-methylbenzimidazole
CB	Cucurbit
TMBQ	Trimethyl-locked benzoquinone
LA	Lactic acid
HA	Hyaluronic acid

## References

- Wang, H.; Jeong, H.Y.; Imura, M.; Wang, L.; Radhakrishnan, L.; Fujita, N.; Castle, T.; Terasaki, O.; Yamauchi, Y. Shape- and size-controlled synthesis in hard templates: Sophisticated chemical reduction for mesoporous monocrystalline platinum nanoparticles. *J. Am. Chem. Soc.* **2011**, *133*, 14526–14529. [[CrossRef](#)] [[PubMed](#)]
- Xu, Y.; Jin, S.; Xu, H.; Nagai, A.; Jiang, D. Conjugated microporous polymers: Design, synthesis and application. *Chem. Soc. Rev.* **2013**, *42*, 8012–8031. [[CrossRef](#)] [[PubMed](#)]
- Lu, A.; Schüth, F. Nanocasting: A versatile strategy for creating nanostructured porous materials. *Adv. Mater.* **2006**, *18*, 1793–1805. [[CrossRef](#)]
- Ishizaki, K.; Komarneni, S.; Nanko, M. *Porous Materials: Process, Technology and Applications*; Springer Science & Business Media: Berlin/Heidelberg, Germany, 2013; Volume 4, ISBN 978-1-4615-5811-8.
- Sher, P.; Ingavle, G.; Ponrathnam, S.; Pawar, A.P. Low density porous carrier based conceptual drug delivery system. *Microporous Mesoporous Mater.* **2007**, *102*, 290–298. [[CrossRef](#)]
- Brownscombe, T.F.; Gergen, W.P.; Bass, R.M.; Mores, M.; Wong, P.K. Process for Preparing Low Density Porous Crosslinked Polymeric Materials. U.S. Patent 5,189,070, 23 February 2003.
- Nagai, K.; Musgrave, C.S.A.A.; Nazarov, W. A Review of Low Density Porous Materials Used in Laser Plasma. *Phys. Plasmas* **2018**, *25*, 30501–30514. [[CrossRef](#)]
- Walcarius, A.; Kuhn, A. Ordered porous thin films in electrochemical analysis. *TrAC-Trends Anal. Chem.* **2008**, *27*, 593–603. [[CrossRef](#)]
- Kitano, M.; Arai, K.; Kodama, A.; Kousaka, T.; Nakajima, K.; Hayashi, S.; Hara, M. Preparation of a sulfonated porous carbon catalyst with high specific surface area. *Catal. Lett.* **2009**, *131*, 242–249. [[CrossRef](#)]
- Velev, O.D.; Lenhoff, A.M. Colloidal crystals as templates for porous materials. *Curr. Opin. Colloid Inter. Sci.* **2000**, *5*, 56–63. [[CrossRef](#)]
- Hsueh, H.Y.; Chen, H.Y.; She, M.S.; Chen, C.K.; Ho, R.M.; Gwo, S.; Hasegawa, H.; Thomas, E.L. Inorganic gyroid with exceptionally low refractive index from block copolymer templating. *Nano Lett.* **2010**, *10*, 4994–5000. [[CrossRef](#)]
- Xi, J.Q.; Ojha, M.; Cho, W.; Plawsky, J.L.; Gill, W.N.; Gessmann, T.; Schubert, E.F. Omnidirectional reflector using nanoporous SiO<sub>2</sub> as a low-refractive-index material. *Opt. Lett.* **2005**, *30*, 1518–1520. [[CrossRef](#)]
- Elimelech, M.; O'Melia, C.R. Kinetics of Deposition of Colloidal Particles in Porous Media. *Environ. Sci. Technol.* **1990**, *24*, 1528–1536. [[CrossRef](#)]
- Millington, R.J.; Quirk, J.P. Permeability of porous solids. *Trans. Faraday Soc.* **1961**, *57*, 1200–1207. [[CrossRef](#)]
- Hollister, S.J. Porous scaffold design for tissue engineering. *Nat. Mater.* **2005**, *4*, 518–524. [[CrossRef](#)]
- Federico, S.; Herzog, W. On the permeability of fibre-reinforced porous materials. *Int. J. Solids Struct.* **2008**, *45*, 2160–2172. [[CrossRef](#)]
- Cui, X.; Chen, K.; Xing, H.; Yang, Q.; Krishna, R.; Bao, Z.; Wu, H.; Zhou, W.; Dong, X.; Han, Y.; et al. Pore chemistry and size control in hybrid porous materials for acetylene capture from ethylene. *Science* **2016**, *353*, 141–144. [[CrossRef](#)]
- Parlett, C.M.A.; Wilson, K.; Lee, A.F. Hierarchical porous materials: Catalytic applications. *Chem. Soc. Rev.* **2013**, *42*, 3876–3893. [[CrossRef](#)] [[PubMed](#)]
- White, R.J.; Luque, R.; Budarin, V.L.; Clark, J.H.; MacQuarrie, D.J. Supported metal nanoparticles on porous materials. Methods and applications. *Chem. Soc. Rev.* **2009**, *38*, 481–494. [[CrossRef](#)]
- Chen, L.; Yang, Y.; Jiang, D. CMPs as scaffolds for constructing porous catalytic frameworks: A built-in heterogeneous catalyst with high activity and selectivity based on nanoporous metalloporphyrin polymers. *J. Am. Chem. Soc.* **2010**, *132*, 9138–9143. [[CrossRef](#)]

21. Galzerano, B.; Capasso, I.; Verdolotti, L.; Lavorgna, M.; Vollaro, P.; Caputo, D.; Iannace, S.; Liguori, B. Design of sustainable porous materials based on 3D-structured silica exoskeletons, Diatomite: Chemico-physical and functional properties. *Mater. Des.* **2018**, *145*, 196–204. [[CrossRef](#)]
22. Guzel Kaya, G.; Yilmaz, E.; Devenci, H. Sustainable nanocomposites of epoxy and silica xerogel synthesized from corn stalk ash: Enhanced thermal and acoustic insulation performance. *Compos. Part B Eng.* **2018**, *150*, 1–6. [[CrossRef](#)]
23. Papa, E.; Medri, V.; Kpogbemabou, D.; Morinière, V.; Laumonier, J.; Vaccari, A.; Rossignol, S. Porosity and insulating properties of silica-fume based foams. *Energy Build.* **2016**, *131*, 223–232. [[CrossRef](#)]
24. Wu, T.; Zhang, P.; Zhang, L.; Wang, J.; Yu, M.; Zhou, X.; Wang, G.G. Relationships between shelter effects and optical porosity: A meta-analysis for tree windbreaks. *Agric. For. Meteorol.* **2018**, *259*, 75–81. [[CrossRef](#)]
25. Das, S.; Heasman, P.; Ben, T.; Qiu, S. Porous Organic Materials: Strategic Design and Structure-Function Correlation. *Chem. Rev.* **2017**, *117*, 1515–1563. [[CrossRef](#)]
26. Talou, M.H.; Camerucci, M.A. Processing of porous mullite ceramics using novel routes by starch consolidation casting. *J. Eur. Ceram. Soc.* **2015**, *35*, 1021–1030. [[CrossRef](#)]
27. Hammel, E.C.; Ighodaro, O.L.R.; Okoli, O.I. Processing and properties of advanced porous ceramics: An application based review. *Ceram. Int.* **2014**, *40*, 15351–15370. [[CrossRef](#)]
28. Song, Q.; Jiang, S.; Hasell, T.; Liu, M.; Sun, S.; Cheetham, A.K.; Sivaniah, E.; Cooper, A.I. Porous organic cage thin films and molecular-sieving membranes. *Adv. Mater.* **2016**, *28*, 2629–2637. [[CrossRef](#)]
29. Sun, M.H.; Huang, S.Z.; Chen, L.H.; Li, Y.; Yang, X.Y.; Yuan, Z.Y.; Su, B.L. Applications of hierarchically structured porous materials from energy storage and conversion, catalysis, photocatalysis, adsorption, separation, and sensing to biomedicine. *Chem. Soc. Rev.* **2016**, *45*, 3479–3563. [[CrossRef](#)]
30. Kewley, A.; Stephenson, A.; Chen, L.; Briggs, M.E.; Hasell, T.; Cooper, A.I. Porous organic cages for gas chromatography separations. *Chem. Mater.* **2015**, *27*, 3207–3210. [[CrossRef](#)]
31. Rouh, H.; Liu, Y.; Katakam, N.; Pham, L.; Zhu, Y.L.; Li, G. Synthesis of Functionalized Chromene and Chroman Derivatives via Cesium Carbonate Promoted Formal [4 + 2] Annulation of 2'-Hydroxychalcones with Allenates. *J. Org. Chem.* **2018**, *83*, 15372–15379. [[CrossRef](#)]
32. Ravikovitch, P.I.; Neimark, A.V. Density functional theory of adsorption in spherical cavities and pore size characterization of templated nanoporous silicas with cubic and three-dimensional hexagonal structures. *Langmuir* **2002**, *18*, 1550–1560. [[CrossRef](#)]
33. Caskey, S.R.; Wong-Foy, A.G.; Matzger, A.J. Dramatic tuning of carbon dioxide uptake via metal substitution in a coordination polymer with cylindrical pores. *J. Am. Chem. Soc.* **2008**, *130*, 10870–10871. [[CrossRef](#)]
34. He, S.; Sun, G.; Cheng, X.; Dai, H.; Chen, X. Nanoporous SiO<sub>2</sub> grafted aramid fibers with low thermal conductivity. *Compos. Sci. Technol.* **2017**, *146*, 91–98. [[CrossRef](#)]
35. Wu, Z.; Zhao, D. Ordered mesoporous materials as adsorbents. *Chem. Commun.* **2011**, *47*, 3332–3338. [[CrossRef](#)] [[PubMed](#)]
36. Taguchi, A.; Schüth, F. Ordered mesoporous materials in catalysis. *Microporous Mesoporous Mater.* **2005**, *77*, 1–45. [[CrossRef](#)]
37. Gulians, V.V.; Carreon, M.A.; Lin, Y.S. Ordered mesoporous and macroporous inorganic films and membranes. *J. Memb. Sci.* **2004**, *235*, 53–72. [[CrossRef](#)]
38. Sarawade, P.B.; Kim, J.-K.; Kim, H.-K.; Kim, H.-T. High specific surface area TEOS-based aerogels with large pore volume prepared at an ambient pressure. *Appl. Surf. Sci.* **2007**, *254*, 574–579. [[CrossRef](#)]
39. Tasciotti, E.; Liu, X.; Bhavane, R.; Plant, K.; Leonard, A.D.; Price, B.K.; Cheng, M.M.C.; Decuzzi, P.; Tour, J.M.; Robertson, F.; et al. Mesoporous silicon particles as a multistage delivery system for imaging and therapeutic applications. *Nat. Nanotechnol.* **2008**, *3*, 151–157. [[CrossRef](#)]
40. Fuertes, A.B. Synthesis of ordered nanoporous carbons of tunable mesopore size by templating SBA-15 silica materials. *Microporous Mesoporous Mater.* **2004**, *67*, 273–281. [[CrossRef](#)]
41. Xu, B.; Xiao, T.; Yan, Z.; Sun, X.; Sloan, J.; González-Cortés, S.L.; Alshahrani, F.; Green, M.L.H. Synthesis of mesoporous alumina with highly thermal stability using glucose template in aqueous system. *Microporous Mesoporous Mater.* **2006**, *91*, 293–295. [[CrossRef](#)]
42. Vinu, A.; Murugesan, V.; Hartmann, M. Pore size engineering and mechanical stability of the cubic mesoporous molecular sieve SBA-1. *Chem. Mater.* **2003**, *15*, 1385–1393. [[CrossRef](#)]
43. Vallet-Regi, M.; Ramila, A.; Del Real, R.P.; Pérez-Pariente, J. A new property of MCM-41: Drug delivery system. *Chem. Mater.* **2001**, *13*, 308–311. [[CrossRef](#)]

44. Chen, H.T.; Trewyn, B.G.; Wiench, J.W.; Pruski, M.; Lin, V.S.Y. Urea and thiourea-functionalized mesoporous silica nanoparticle catalysts with enhanced catalytic activity for diels-alder reaction. *Top. Catal.* **2010**, *53*, 187–191. [[CrossRef](#)]
45. Verma, P.; Kuwahara, Y.; Mori, K.; Yamashita, H. Pd/Ag and Pd/Au bimetallic nanocatalysts on mesoporous silica for plasmon-mediated enhanced catalytic activity under visible light irradiation. *J. Mater. Chem. A* **2016**, *4*, 10142–10150. [[CrossRef](#)]
46. Ahuja, G.; Pathak, K. Porous carriers for controlled/modulated drug delivery. *Indian J. Pharm. Sci.* **2009**, *71*, 599–607. [[CrossRef](#)] [[PubMed](#)]
47. Malik, D.J.; Webb, C.; Holdich, R.G.; Ramsden, J.J.; Warwick, G.L.; Roche, I.; Williams, D.J.; Trochimczuk, A.W.; Dale, J.A.; Hoenich, N.A. Synthesis and characterization of size-selective nanoporous polymeric adsorbents for blood purification. *Sep. Purif. Technol.* **2009**, *66*, 578–585. [[CrossRef](#)]
48. Van Speybroeck, M.; Barillaro, V.; Thi, T.D.; Mellaerts, R.; Martens, J.; Van Humbeeck, J.; Vermant, J.; Annaert, P.; Van Den Mooter, G.; Augustijns, P. Ordered mesoporous silica material SBA-15: A broad-spectrum formulation platform for poorly soluble drugs. *J. Pharm. Sci.* **2009**, *98*, 2648–2658. [[CrossRef](#)]
49. Naik, B.; Ghosh, N. A Review on Chemical Methodologies for Preparation of Mesoporous Silica and Alumina Based Materials. *Recent Pat. Nanotechnol.* **2009**, *3*, 213–224. [[CrossRef](#)]
50. Trewyn, B.G.; Slowing, I.I.; Giri, S.; Chen, H.T.; Lin, V.S.Y. Synthesis and functionalization of a mesoporous silica nanoparticle based on the sol-gel process and applications in controlled release. *Acc. Chem. Res.* **2007**, *40*, 846–853. [[CrossRef](#)]
51. Heikkilä, T.; Salonen, J.; Tuura, J.; Hamdy, M.S.; Mul, G.; Kumar, N.; Salmi, T.; Murzin, D.Y.; Laitinen, L.; Kaukonen, A.M.; et al. Mesoporous silica material TUD-1 as a drug delivery system. *Int. J. Pharm.* **2007**, *331*, 133–138. [[CrossRef](#)]
52. Zhu, Y.; Shi, J.; Chen, H.; Shen, W.; Dong, X. A facile method to synthesize novel hollow mesoporous silica spheres and advanced storage property. *Microporous Mesoporous Mater.* **2005**, *84*, 218–222. [[CrossRef](#)]
53. Björk, E.M.; Militello, M.P.; Tamborini, L.H.; Coneo Rodriguez, R.; Planes, G.A.; Acevedo, D.F.; Moreno, M.S.; Odén, M.; Barbero, C.A. Mesoporous silica and carbon based catalysts for esterification and biodiesel fabrication—The effect of matrix surface composition and porosity. *Appl. Catal. A Gen.* **2017**, *533*, 49–58. [[CrossRef](#)]
54. Siefker, J.; Karande, P.; Coppens, M.O. Packaging biological cargoes in mesoporous materials: Opportunities for drug delivery. *Expert Opin. Drug Deliv.* **2014**, *11*, 1781–1793. [[CrossRef](#)]
55. Liu, C.; Wang, X.; Lee, S.; Pfefferle, L.D.; Haller, G.L. Surfactant chain length effect on the hexagonal-to-cubic phase transition in mesoporous silica synthesis. *Microporous Mesoporous Mater.* **2012**, *147*, 242–251. [[CrossRef](#)]
56. Hassanzadeh, S.; Khoee, S.; Firoozpour, L. Effect of the copolymerized aromatic and unsaturated monomers on the affinity of drug-polyesters in the core-shell nanoparticles. *Macromol. Res.* **2013**, *21*, 55–64. [[CrossRef](#)]
57. Khoee, S.; Sattari, A.; Atyabi, F. Physico-chemical properties investigation of cisplatin loaded polybutyladipate (PBA) nanoparticles prepared by w/o/w. *Mater. Sci. Eng. C* **2012**, *32*, 1078–1086. [[CrossRef](#)]
58. Erdodi, G.; Kennedy, J.P. Amphiphilic conetworks: Definition, synthesis, applications. *Prog. Polym. Sci.* **2006**, *31*, 1–18. [[CrossRef](#)]
59. Beck, J.S.; Vartuli, J.C.; Roth, W.J.; Leonowicz, M.E.; Kresge, C.T.; Schmitt, K.D.; Chu, C.T.W.; Olson, D.H.; Sheppard, E.W.; McCullen, S.B.; et al. A New Family of Mesoporous Molecular Sieves Prepared with Liquid Crystal Templates. *J. Am. Chem. Soc.* **1992**, *114*, 10834–10843. [[CrossRef](#)]
60. Makowski, P.; Deschanel, X.; Grandjean, A.; Meyer, D.; Toquer, G.; Goettmann, F. Mesoporous materials in the field of nuclear industry: Applications and perspectives. *N. J. Chem.* **2012**, *36*, 531–541. [[CrossRef](#)]
61. Munoz, B.; Ramila, A.; Perez-Pariente, J.; Diaz, I.; Vallet-Regi, M. MCM-41 organic modification as drug delivery rate regulator. *Chem. Mater.* **2003**, *15*, 500–503. [[CrossRef](#)]
62. Tanev, P.T.; Pinnavaia, T.J. Mesoporous silica molecular sieves prepared by ionic and neutral surfactant templating: A comparison of physical properties. *Chem. Mater.* **1996**, *8*, 2068–2079. [[CrossRef](#)]
63. Lin, H.P.; Mou, C.Y. Structural and Morphological Control of Cationic Surfactant-Templated Mesoporous Silica. *Acc. Chem. Res.* **2002**, *35*, 927–935. [[CrossRef](#)]
64. Brown, J.; Richer, R.; Mercier, L. One-step synthesis of high capacity mesoporous Hg<sup>2+</sup> adsorbents by non-ionic surfactant assembly. *Microporous Mesoporous Mater.* **2000**, *37*, 41–48. [[CrossRef](#)]
65. Hato, M.; Yamashita, J.; Shiono, M. Aqueous phase behavior of lipids with isoprenoid type hydrophobic chains. *J. Phys. Chem. B* **2009**, *113*, 10196–10209. [[CrossRef](#)]

66. Taylor, D.J.F.; Thomas, R.K.; Li, P.X.; Penfold, J. Adsorption of oppositely charged polyelectrolyte/surfactant mixtures. Neutron reflection from alkyl trimethylammonium bromides and sodium poly(styrenesulfonate) at the air/water interface: The effect of surfactant chain length. *Langmuir* **2003**, *19*, 3712–3719. [[CrossRef](#)]
67. Lockwood, N.A.; De Pablo, J.J.; Abbott, N.L. Influence of surfactant tail branching and organization on the orientation of liquid crystals at aqueous-liquid crystal interfaces. *Langmuir* **2005**, *21*, 6805–6814. [[CrossRef](#)] [[PubMed](#)]
68. Jinno, J.; Oh, D.; Crison, J.R.; Amidon, G.L. Dissolution of Ionizable Water-Insoluble Drugs: The Combined Effect of pH and Surfactant. *J. Pharm. Sci.* **2000**, *89*, 268–274. [[CrossRef](#)]
69. Hua, X.Y.; Rosen, M.J. Dynamic surface tension of aqueous surfactant solutions. I. Basic parameters. *J. Colloid Interface Sci.* **1988**, *124*, 652–659. [[CrossRef](#)]
70. Li, W.; Xie, D.; Song, B.; Feng, L.; Pei, X.; Cui, Z. Synthesis and characterization of ordered mesoporous silica using rosin-based Gemini surfactants. *J. Mater. Sci.* **2018**, *53*, 2434–2442. [[CrossRef](#)]
71. Li, M.; Zhang, C.; Yang, X.L.; Xu, H.B. Controllable synthesis of hollow mesoporous silica nanoparticles templated by kinetic self-assembly using a gemini surfactant. *RSC Adv.* **2013**, *3*. [[CrossRef](#)]
72. Niu, D.; Ma, Z.; Li, Y.; Shi, J. Synthesis of Core-Shell Structured Dual-Mesoporous Silica Spheres with Tunable Pore Size and Controllable Shell Thickness. *J. Am. Chem. Soc.* **2010**, *132*, 15144–15147. [[CrossRef](#)]
73. Yang, J.; Chen, W.; Ran, X.; Wang, W.; Fan, J.; Zhang, W. Boric acid assisted formation of mesostructured silica: From hollow spheres to hierarchical assembly. *RSC Adv.* **2014**, *4*, 20069–20076. [[CrossRef](#)]
74. Blin, J.L.; Léonard, A.; Su, B.L. Synthesis of Large Pore Disordered MSU-Type Mesoporous Silicas through the Assembly of C16(EO)10 Surfactant and TMOS Silica Source: Effect of the Hydrothermal Treatment and Thermal Stability of Materials. *J. Phys. Chem. B* **2001**, *105*, 6070–6079. [[CrossRef](#)]
75. Liu, J.; Yang, Q.; Zhao, X.S.; Zhang, L. Pore size control of mesoporous silicas from mixtures of sodium silicate and TEOS. *Microporous Mesoporous Mater.* **2007**, *106*, 62–67. [[CrossRef](#)]
76. Kleitz, F.; Marlow, F.; Stucky, G.D.; Schüth, F. Mesoporous Silica Fibers: Synthesis, Internal Structure, and Growth Kinetics. *Chem. Mater.* **2001**, *13*, 3587–3595. [[CrossRef](#)]
77. Linssen, T.; Cassiers, K.; Cool, P.; Vansant, E. Mesoporous templated silicates: An overview of their synthesis, catalytic activation and evaluation of the stability. *Adv. Colloid Interface Sci.* **2003**, *103*, 121–147. [[CrossRef](#)]
78. Abdelbasir, S.M.; El-Sheikh, S.M.; Rashad, M.M.; Rayan, D.A. Controlling the Optical and Magnetic Properties of Nanostructured Cuprous Oxide Synthesized from Waste Electric Cables. *Electron. Mater. Lett.* **2018**, *14*, 505–516. [[CrossRef](#)]
79. Khalil, R.A.; Zarari, A.A. Theoretical estimation of the critical packing parameter of amphiphilic self-assembled aggregates. *Appl. Surf. Sci.* **2014**, *318*, 85–89. [[CrossRef](#)]
80. Lebedev, O.I.; Van Tendeloo, G.; Collart, O.; Cool, P.; Vansant, E.F. Structure and microstructure of nanoscale mesoporous silica spheres. *Solid State Sci.* **2004**, *6*, 489–498. [[CrossRef](#)]
81. Cauda, V.; Argyo, C.; Piercey, D.G.; Bein, T. “Liquid-Phase Calcination” of Colloidal Mesoporous Silica Nanoparticles in High-Boiling Solvents. *J. Am. Chem. Soc.* **2011**, *133*, 6484–6486. [[CrossRef](#)]
82. Han, L.; Gao, C.; Wu, X.; Chen, Q.; Shu, P.; Ding, Z.; Che, S. Anionic surfactants templating route for synthesizing silica hollow spheres with different shell porosity. *Solid State Sci.* **2011**, *13*, 721–728. [[CrossRef](#)]
83. Ågren, P.; Lindén, M.; Rosenholm, J.B.; Schwarzenbacher, R.; Kriechbaum, M.; Amenitsch, H.; Lagner, P.; Blanchard, J.; Schüth, F. Kinetics of Cosurfactant–Surfactant–Silicate Phase Behavior. 1. Short-Chain Alcohols. *J. Phys. Chem. B* **1999**, *103*, 5943–5948. [[CrossRef](#)]
84. He, Q.; Cui, X.; Cui, F.; Guo, L.; Shi, J. Size-controlled synthesis of monodispersed mesoporous silica nano-spheres under a neutral condition. *Microporous Mesoporous Mater.* **2009**, *117*, 609–616. [[CrossRef](#)]
85. Yu, J.; Shi, J.L.; Chen, H.R.; Yan, J.N.; Yan, D.S. Effect of inorganic salt addition during synthesis on pore structure and hydrothermal stability of mesoporous silica. *Microporous Mesoporous Mater.* **2001**, *46*, 153–162. [[CrossRef](#)]
86. Luechinger, M.; Pirngruber, G.D.; Lindlar, B.; Lagner, P.; Prins, R. The effect of the hydrophobicity of aromatic swelling agents on pore size and shape of mesoporous silicas. *Microporous Mesoporous Mater.* **2005**, *79*, 41–52. [[CrossRef](#)]
87. Weres, O.; Yee, A.; Tsao, L. Kinetics of silica polymerization. *J. Colloid Interface Sci.* **1981**, *84*, 379–402. [[CrossRef](#)]
88. Lin, H.P.; Tsai, C.P. Synthesis of Mesoporous Silica Nanoparticles from a Low-concentration CnTMAX-Sodium Silicate Components. *Chem. Lett.* **2003**, *32*, 1092–1093. [[CrossRef](#)]

89. Niederberger, M.; Pinna, N. *Metal. Oxide Nanoparticles in Organic Solvents; Engineering Materials and Processes*; Springer: London, UK, 2009; ISBN 978-1-84882-670-0.
90. Faustini, M.; Nicole, L.; Ruiz-Hitzky, E.; Sanchez, C. History of Organic-Inorganic Hybrid Materials: Prehistory, Art, Science, and Advanced Applications. *Adv. Funct. Mater.* **2018**, *28*. [[CrossRef](#)]
91. AlOthman, Z. A Review: Fundamental Aspects of Silicate Mesoporous Materials. *Materials (Basel)* **2012**, *5*, 2874–2902. [[CrossRef](#)]
92. Léonard, A.; Blin, J.L.; Jacobs, P.A.; Grange, P.; Su, B.L. Chemistry of silica at different concentrations of non-ionic surfactant solutions: Effect of pH of the synthesis gel on the preparation of mesoporous silicas. *Microporous Mesoporous Mater.* **2003**, *63*, 59–73. [[CrossRef](#)]
93. Sadegh, H.; Gomaa, A.M.A.; Hamid, J.N.; Zahra, M. Nanomaterial Surface Modifications for Enhancement of the Pollutant Adsorption From Wastewater: Adsorption of Nanomaterials. *Nanotechnol. Environ. Eng.* **2019**, 143–170.
94. Ding, X.; Tan, F.; Zhao, H.; Hua, M.; Wang, M.; Xin, Q.; Zhang, Y. Enhancing gas permeation and separation performance of polymeric membrane by incorporating hollow polyamide nanoparticles with dense shell. *J. Memb. Sci.* **2019**, *570–571*, 53–60. [[CrossRef](#)]
95. Cho, A.; Byun, S.; Kim, B.M. AuPd–Fe<sub>3</sub>O<sub>4</sub> Nanoparticle Catalysts for Highly Selective, One-Pot Cascade Nitro-Reduction and Reductive Amination. *Adv. Synth. Catal.* **2018**, *360*, 1253–1261. [[CrossRef](#)]
96. Liu, Y.; Peng, G.; Jixiang, W.; Zhishu, Y.; Huidan, L.; Jiefeng, H.; Zhenhuan, L.; Dayong, F.; Ming, L. In-situ ion-exchange synthesis Ag<sub>2</sub>S modified SnS<sub>2</sub> nanosheets toward highly photocurrent response and photocatalytic activity. *J. Colloid Interface Sci.* **2018**, *512*, 784–791. [[CrossRef](#)] [[PubMed](#)]
97. Baranik, A.; Gagor, A.; Queralt, I.; Marguí, E.; Sitko, R.; Zawisza, B. Ceria nanoparticles deposited on graphene nanosheets for adsorption of copper(II) and lead(II) ions and of anionic species of arsenic and selenium. *Microchim. Acta* **2018**, *185*, 264. [[CrossRef](#)]
98. Ghaemi, N.; Madaeni, S.S.; Daraei, P.; Rajabi, H.; Zinadini, S.; Alizadeh, A.; Heydari, R.; Beygzadeh, M.; Ghouzivand, S. Polyethersulfone membrane enhanced with iron oxide nanoparticles for copper removal from water: Application of new functionalized Fe<sub>3</sub>O<sub>4</sub> nanoparticles. *Chem. Eng. J.* **2015**, *263*, 101–112. [[CrossRef](#)]
99. Puay, N.Q.; Qiu, G.; Ting, Y.P. Effect of Zinc oxide nanoparticles on biological wastewater treatment in a sequencing batch reactor. *J. Clean. Prod.* **2015**, *88*, 139–145. [[CrossRef](#)]
100. Kayvani-Fard, A.; Rhadfi, T.; Mckay, G.; Al-marri, M.; Abdala, A.; Hilal, N.; Hussien, M.A. Enhancing oil removal from water using ferric oxide nanoparticles doped carbon nanotubes adsorbents. *Chem. Eng. J.* **2016**, *293*, 90–101. [[CrossRef](#)]
101. Markandeya, S.; Mohan, D. Toxicity of Disperse Dyes and its Removal from Wastewater Using Various Adsorbents: A Review. *Res. J. Environ. Toxicol.* **2017**, *11*, 72–89. [[CrossRef](#)]
102. Marahel, F.; Ghaedi, M.; Nasiri Kokhdan, S. Silver nanoparticle loaded on activated carbon as an adsorbent for the removal of Sudan Red 7B from aqueous solution. *Fresenius Environ. Bull.* **2012**, *21*, 163–170.
103. Kadirvelu, K.; Kavipriya, M.; Karthika, C.; Radhika, M.; Vennilamani, N.; Patabhi, S. Utilization of various agricultural wastes for activated carbon preparation and application for the removal of dyes and metal ions from aqueous solutions. *Bioresour. Technol.* **2003**, *87*, 129–132. [[CrossRef](#)]
104. Armağan, B.; Özdemir, O.; Turan, M.; Çelik, M. The removal of reactive azo dyes by natural and modified zeolites. *J. Chem. Technol. Biotechnol.* **2003**, *78*, 725–732. [[CrossRef](#)]
105. Daraei, P.; Madaeni, S.S.; Salehi, E.; Ghaemi, N.; Ghari, H.S.; Khadivi, M.A.; Rostami, E. Novel thin film composite membrane fabricated by mixed matrix nanoclay/chitosan on PVDF microfiltration support: Preparation, characterization and performance in dye removal. *J. Memb. Sci.* **2013**, *436*, 97–108. [[CrossRef](#)]
106. Luo, X.; Zhan, Y.; Huang, Y.; Yang, L.; Tu, X.; Luo, S. Removal of water-soluble acid dyes from water environment using a novel magnetic molecularly imprinted polymer. *J. Hazard. Mater.* **2011**, *187*, 274–282. [[CrossRef](#)] [[PubMed](#)]
107. Aguado, J.; Arsuaga, J.M.; Arencibia, A.; Lindo, M.; Gascón, V. Aqueous heavy metals removal by adsorption on amine-functionalized mesoporous silica. *J. Hazard. Mater.* **2009**, *163*, 213–221. [[CrossRef](#)]
108. Anbia, M.; Hariri, S.A. Removal of methylene blue from aqueous solution using nanoporous SBA-3. *Desalination* **2010**, *261*, 61–66. [[CrossRef](#)]

109. Haque, E.; Jun, J.W.; Jhung, S.H. Adsorptive removal of methyl orange and methylene blue from aqueous solution with a metal-organic framework material, iron terephthalate (MOF-235). *J. Hazard. Mater.* **2011**, *185*, 507–511. [[CrossRef](#)]
110. Dadfarnia, S.; Haji Shabani, A.M.; Moradi, S.E.; Emami, S. Methyl red removal from water by iron based metal-organic frameworks loaded onto iron oxide nanoparticle adsorbent. *Appl. Surf. Sci.* **2015**, *330*, 85–93. [[CrossRef](#)]
111. Bulut, E.; Özacar, M.; Şengil, İ.A. Adsorption of malachite green onto bentonite: Equilibrium and kinetic studies and process design. *Microporous Mesoporous Mater.* **2008**, *115*, 234–246. [[CrossRef](#)]
112. Vojoudi, H.; Badiei, A.; Amiri, A.; Banaei, A.; Ziarani, G.M.; Schenk-Joß, K. Efficient device for the benign removal of organic pollutants from aqueous solutions using modified mesoporous magnetite nanostructures. *J. Phys. Chem. Solids* **2018**, *113*, 210–219. [[CrossRef](#)]
113. Bruzzoniti, M.C.; Prella, A.; Sarzanini, C.; Onida, B.; Fiorilli, S.; Garrone, E. Retention of heavy metal ions on SBA-15 mesoporous silica functionalised with carboxylic groups. *J. Sep. Sci.* **2007**, *30*, 2414–2420. [[CrossRef](#)]
114. Veisi, H.; Razeghi, S.; Mohammadi, P.; Hemmati, S. Silver nanoparticles decorated on thiol-modified magnetite nanoparticles (Fe<sub>3</sub>O<sub>4</sub>/SiO<sub>2</sub>-Pr-S-Ag) as a recyclable nanocatalyst for degradation of organic dyes. *Mater. Sci. Eng. C* **2019**, *97*, 624–631. [[CrossRef](#)] [[PubMed](#)]
115. Ho, K.Y.; McKay, G.; Yeung, K.L. Selective Adsorbents from Ordered Mesoporous Silica. *Langmuir* **2003**, *19*, 3019–3024. [[CrossRef](#)]
116. Zhang, M.; Zhu, W.; Li, H.; Xun, S.; Ding, W.; Liu, J.; Zhao, Z.; Wang, Q. One-pot synthesis, characterization and desulfurization of functional mesoporous W-MCM-41 from POM-based ionic liquids. *Chem. Eng. J.* **2014**, *243*, 386–393. [[CrossRef](#)]
117. Tuong, T.; Tran, V.; Kongparakul, S.; Karnjanakom, S.; Reubroycharoen, P. Highly productive xylose dehydration using a sulfonic acid functionalized KIT-6 catalyst. *Fuel* **2019**, *236*, 1156–1163. [[CrossRef](#)]
118. Uson, L.; Hueso, J.L.; Sebastian, V.; Arenal, R.; Florea, I.; Irusta, S.; Arruebo, M.; Santamaria, J. In-situ preparation of ultra-small Pt nanoparticles within rod-shaped mesoporous silica particles: 3-D tomography and catalytic oxidation of n-hexane. *Catal. Commun.* **2017**, *100*, 93–97. [[CrossRef](#)]
119. Cruz, P.; Pérez, Y.; del Hierro, I. Titanium alkoxides immobilized on magnetic mesoporous silica nanoparticles and their characterization by solid state voltammetry techniques: Application in ring opening polymerization. *Microporous Mesoporous Mater.* **2017**, *240*, 227–235. [[CrossRef](#)]
120. Jing, Z.C.; Cao, H.C.; Song, W. Having it both ways: Delicate hierarchical structure and robust mechanical stability on micro / nanomaterials with mesoporous silica coating. *J. Porous Mater.* **2016**. [[CrossRef](#)]
121. Fan, C.; Huang, B.; Pan, C.; Zhang, J.; Wen, H.; Yang, J.; Sun, Y. Synthesis of flake-like mesoporous silicate having multiple metal centers and catalytic application for conversion of D(-)-fructose into fine chemicals. *Mater. Chem. Phys.* **2017**, *200*, 295–307. [[CrossRef](#)]
122. Hao, N.; Chorsi, H.T.; Zhang, J.X.J. Hierarchical Lotus Leaf-Like Mesoporous Silica Material with Unique Bilayer and Hollow Sandwich-Like Folds: Synthesis, Mechanism, and Applications. *ACS Sustain. Chem. Eng.* **2017**, *5*, 2044–2049. [[CrossRef](#)]
123. Snoussi, Y.; Bastide, S.; Abderrabba, M.; Chehimi, M.M. Sonochemical synthesis of Fe<sub>3</sub>O<sub>4</sub>@NH<sub>2</sub>-mesoporous silica@Polypyrrole/Pd: A core/double shell nanocomposite for catalytic applications. *Ultrason. Sonochem.* **2018**, *41*, 551–561. [[CrossRef](#)]
124. Jiao, J.; Fu, J.; Wei, Y.; Zhao, Z.; Duan, A.; Xu, C.; Li, J.; Song, H.; Zheng, P.; Wang, X.; et al. Al-modified dendritic mesoporous silica nanospheres-supported NiMo catalysts for the hydrodesulfurization of dibenzothiophene: Efficient accessibility of active sites and suitable metal-support interaction. *J. Catal.* **2017**, *356*, 269–282. [[CrossRef](#)]
125. Xia, X.; Meng, J.; Wu, H.; Cheng, T.; Liu, G. Integration of multiple active sites on large-pore mesoporous silica for enantioselective tandem reactions. *Chem. Commun.* **2017**, *53*, 1638–1641. [[CrossRef](#)] [[PubMed](#)]
126. Xu, W.; Ollevier, T.; Kleitz, F. Iron-Modified Mesoporous Silica as an Efficient Solid Lewis Acid Catalyst for the Mukaiyama Aldol Reaction. *ACS Catal.* **2018**, *8*, 1932–1944. [[CrossRef](#)]
127. Padwa, A. *1,3-Dipolar Cycloaddition Chemistry. Volumes 1 and 2*; Padwa, A., Ed.; John Wiley and Sons: New York, NY, USA, 1986; Volume 23.
128. Rao, J.N.S.; Raghunathan, R. An expedient diastereoselective synthesis of pyrrolidinyli spirooxindoles fused to sugar lactone via [3+2] cycloaddition of azomethine ylides. *Tetrahedron Lett.* **2012**, *53*, 854–858. [[CrossRef](#)]

129. Alvarez, R.; Velazquez, S.; San-Felix, A.; Aquaro, S.; Clercq, E.D.; Perno, C.F.; Karlsson, A.; Balzarini, J.; Camarasa, M.J. 1,2,3-Triazole-[2,5-Bis-O-(tert-butyl(dimethylsilyl)-beta.-D-ribofuranosyl]-3'-spiro-5''-(4''-amino-1'', 2''-oxathiole 2'',2''-dioxide) (TSAO) Analogs: Synthesis and Anti-HIV-1 Activity. *J. Med. Chem.* **1994**, *37*, 4185–4194. [[CrossRef](#)]
130. da Silva, F.d.C.; de Souza, M.C.B.V.; Frugulhetti, I.I.P.; Castro, H.C.; Souza, S.L.d.O.; de Souza, T.M.L.; Rodrigues, D.Q.; Souza, A.M.T.; Abreu, P.A.; Passamani, F. Synthesis, HIV-RT inhibitory activity and SAR of 1-benzyl-1H-1,2,3-triazole derivatives of carbohydrates. *Eur. J. Med. Chem.* **2009**, *44*, 373–383. [[CrossRef](#)]
131. Fung-Tomc, J.C.; Huczko, E.; Minassian, B.; Bonner, D.P. In vitro activity of a new oral triazole, BMS-207147 (ER-30346). *Antimicrob. Agents Chemother.* **1998**, *42*, 313–318. [[CrossRef](#)] [[PubMed](#)]
132. Buckle, D.R.; Rockell, C.J.; Smith, H.; Spicer, B.A. Studies on 1,2,3-triazoles. 13. (Piperazinylalkoxy) [1]benzopyrano[2,3-d]-1,2,3-triazol-9(1H)-ones with combined H1-antihistamine and mast cell stabilizing properties. *J. Med. Chem.* **1986**, *29*, 2262–2267. [[CrossRef](#)]
133. Hoshino, M. Effect of 3-Amino-1,2,4-triazole on the Experimental Production of Liver Cancer. *Nature* **1960**, *186*, 174–175. [[CrossRef](#)]
134. Thompson, A.M.; Blaser, A.; Anderson, R.F.; Shinde, S.S.; Franzblau, S.G.; Ma, Z.; Denny, W.A.; Palmer, B.D. Synthesis, Reduction Potentials, and Antitubercular Activity of Ring A/B Analogues of the Bioreductive Drug (6S)-2-Nitro-6-[[4-(trifluoromethoxy)benzyl]oxy]-6,7-dihydro-5H-imidazo[2,1-b][1,3]oxazine (PA-824). *J. Med. Chem.* **2009**, *52*, 637–645. [[CrossRef](#)]
135. Jordão, A.K.; Ferreira, V.F.; Lima, E.S.; de Souza, M.C.B.V.; Carlos, E.C.L.; Castro, H.C.; Geraldo, R.B.; Rodrigues, C.R.; Almeida, M.C.B.; Cunha, A.C. Synthesis, antiplatelet and in silico evaluations of novel N-substituted-phenylamino-5-methyl-1H-1,2,3-triazole-4-carbohydrazides. *Bioorg. Med. Chem.* **2009**, *17*, 3713–3719. [[CrossRef](#)]
136. Hou, D.R.; Alam, S.; Kuan, T.C.; Ramanathan, M.; Lin, T.P.; Hung, M.S. 1,2,3-Triazole derivatives as new cannabinoid CB1 receptor antagonists. *Bioorg. Med. Chem. Lett.* **2009**, *19*, 1022–1025. [[CrossRef](#)] [[PubMed](#)]
137. Shen, J.; Woodward, R.; Kedenburg, J.P.; Liu, X.; Chen, M.; Fang, L.; Sun, D.; Wang, P.G. Histone Deacetylase Inhibitors through Click Chemistry. *J. Med. Chem.* **2008**, *51*, 7417–7427. [[CrossRef](#)]
138. Wendlandt, A.E.; Suess, A.M.; Stahl, S.S. Copper-catalyzed aerobic oxidative C-H functionalizations: Trends and mechanistic insights. *Angew. Chem.-Int. Ed.* **2011**, *50*, 11062–11087. [[CrossRef](#)]
139. Nasr-Esfahani, M.; Mohammadpoor-Baltork, I.; Khosropour, A.R.; Moghadam, M.; Mirkhani, V.; Tangestaninejad, S. Synthesis and characterization of Cu(II) containing nanosilica triazine dendrimer: A recyclable nanocomposite material for the synthesis of benzimidazoles, benzothiazoles, bis-benzimidazoles and bis-benzothiazoles. *J. Mol. Catal. A Chem.* **2013**, *379*, 243–254. [[CrossRef](#)]
140. Bahadorikhali, S.; Ma'mani, L.; Mahdavi, H.; Shafiee, A. Copper supported B-cyclodextrin functionalized PEGylated mesoporous silica nanoparticle -graphene oxide hybrid: An efficient and recyclable nano-catalyst for straightforward synthesis of 2-arylbenzimidazoles and 1,2,3-triazoles. *Microporous Mesoporous Mater.* **2018**, *262*, 207–216. [[CrossRef](#)]
141. Bhadra, M.; Sasmal, H.S.; Basu, A.; Midya, S.P.; Kandambeth, S.; Pachfule, P.; Balaraman, E.; Banerjee, R. Predesigned Metal-Anchored Building Block for in Situ Generation of Pd Nanoparticles in Porous Covalent Organic Framework: Application in Heterogeneous Tandem Catalysis. *ACS Appl. Mater. Interfaces* **2017**, *9*, 13785–13792. [[CrossRef](#)]
142. Sobocinski, J.; Laure, W.; Taha, M.; Courcot, E.; Chai, F.; Simon, N.; Addad, A.; Martel, B.; Haulon, S.; Woisel, P.; et al. Mussel inspired coating of a biocompatible cyclodextrin based polymer onto CoCr vascular stents. *ACS Appl. Mater. Interfaces* **2014**, *6*, 3575–3586. [[CrossRef](#)] [[PubMed](#)]
143. Takahashi, K. Reactions Mediated by Cyclodextrins. *Mol. Encapsulation Org. React. Constrained Syst.* **2010**, *98*, 91–115.
144. Hassanzadeh, S.; Khoee, S. Influence of the polymer structure on the drug-polymer interactions in the micellar nanoparticles: Mixed homopolymer and copolymerized cores. *J. Appl. Polym. Sci.* **2013**, *129*, 652–664. [[CrossRef](#)]
145. Sreejith, S.; Ma, X.; Zhao, Y. Graphene oxide wrapping on squaraine-loaded mesoporous silica nanoparticles for bioimaging. *J. Am. Chem. Soc.* **2012**, *134*, 17346–17349. [[CrossRef](#)]
146. Shang, L.; Bian, T.; Zhang, B.; Zhang, D.; Wu, L.Z.; Tung, C.H.; Yin, Y.; Zhang, T. Graphene-supported ultrafine metal nanoparticles encapsulated by mesoporous silica: Robust catalysts for oxidation and reduction reactions. *Angew. Chem.-Int. Ed.* **2014**, *53*, 250–254. [[CrossRef](#)]



147. Wang, Y.; Wang, K.; Zhao, J.; Liu, X.; Bu, J.; Yan, X.; Huang, R. Multifunctional mesoporous silica-coated graphene nanosheet used for chemo-photothermal synergistic targeted therapy of glioma. *J. Am. Chem. Soc.* **2013**, *135*, 4799–4804. [[CrossRef](#)]
148. Schedin, F.; Geim, A.K.; Morozov, S.V.; Hill, E.W.; Blake, P.; Katsnelson, M.I.; Novoselov, K.S. Acute toxic effects of drug abuse: Diagnosis and treatment. *J. Fla. Med. Assoc.* **1971**, *58*, 41–42. [[CrossRef](#)]
149. Kazemnejadi, M.; Sardarian, A.R. Ecofriendly synthesis of a heterogeneous polyvinyl alcohol immobilized copper(II) Schiff base complex as an efficient, reusable catalyst for the one-pot three-component green preparation of 5-substituted 1H-tetrazoles under mild conditions. *RSC Adv.* **2016**, *6*, 91999–92006. [[CrossRef](#)]
150. Sharghi, H.; Ebrahimpourmoghaddam, S.; Doroodmand, M.M. Facile synthesis of 5-substituted-1H-tetrazoles and 1-substituted-1H-tetrazoles catalyzed by recyclable 4'-phenyl-2,2':6',2''-terpyridine copper(II) complex immobilized onto activated multi-walled carbon nanotubes. *J. Organomet. Chem.* **2013**, *738*, 41–48. [[CrossRef](#)]
151. Sardarian, A.R.; Eslahi, H.; Esmaeilpour, M. Copper(II) Complex Supported on Fe<sub>3</sub>O<sub>4</sub>@SiO<sub>2</sub> Coated by Polyvinyl Alcohol as Reusable Nanocatalyst in N-Arylation of Amines and N(H)- Heterocycles and Green Synthesis of 1H-Tetrazoles. *Chem. Sel.* **2018**, *3*, 1499–1511. [[CrossRef](#)]
152. Anbarasan, P.; Schareina, T.; Beller, M. Recent developments and perspectives in palladium-catalyzed cyanation of aryl halides: Synthesis of benzonitriles. *Chem. Soc. Rev.* **2011**, *40*, 5049–5067. [[CrossRef](#)] [[PubMed](#)]
153. Molnár, A. Efficient, Selective, and Recyclable Palladium Catalysts in Carbon-Carbon Coupling Reactions. *Chem. Rev.* **2011**, *111*, 2251–2320. [[CrossRef](#)]
154. Phan, N.T.S.; Van Der Sluys, M.; Jones, C.W. On the nature of the active species in palladium catalyzed Mizoroki-Heck and Suzuki-Miyaura couplings-Homogeneous or heterogeneous catalysis, a critical review. *Adv. Synth. Catal.* **2006**, *348*, 609–679. [[CrossRef](#)]
155. Seganish, W.M.; Mowery, M.E.; Riggleman, S.; DeShong, P. Palladium-catalyzed homocoupling of aryl halides in the presence of fluoride. *Tetrahedron* **2005**, *61*, 2117–2121. [[CrossRef](#)]
156. Magano, J.; Dunetz, J.R. Large-Scale Applications of Transition Metal-Catalyzed Couplings for the Synthesis of Pharmaceuticals. *Chem. Rev.* **2011**, *111*, 2177–2250. [[CrossRef](#)]
157. Corbet, J.P.; Mignani, G. Selected Patented Cross-Coupling Reaction Technologies. *Chem. Rev.* **2006**, *106*, 2651–2710. [[CrossRef](#)]
158. Geun, S.C.; Suk, B.Y.; Jung, H.K.; Yu, J.S. Spherical carbon capsules with hollow macroporous core and mesoporous shell structures as a highly efficient catalyst support in the direct methanol fuel cell. *Chem. Commun.* **2004**, 2766–2767. [[CrossRef](#)]
159. Mosaddegh, N.; Yavari, I. Pd-poly(N-vinyl-2-pyrrolidone)/MCM-48 nanocomposite: A novel catalyst for the Ullmann reaction. *Chem. Pap.* **2018**, *72*, 2013–2021. [[CrossRef](#)]
160. Tan, S.Y.; Teh, C.; Ang, C.Y.; Li, M.; Li, P.; Korzh, V.; Zhao, Y. Responsive mesoporous silica nanoparticles for sensing of hydrogen peroxide and simultaneous treatment toward heart failure. *Nanoscale* **2017**, *9*, 2253–2261. [[CrossRef](#)] [[PubMed](#)]
161. Hou, L.; Zheng, Y.; Wang, Y.; Hu, Y.; Shi, J.; Liu, Q.; Zhang, H.; Zhang, Z. Self-Regulated Carboxyphenylboronic Acid-Modified Mesoporous Silica Nanoparticles with “touch Switch” Releasing Property for Insulin Delivery. *ACS Appl. Mater. Interfaces* **2018**, *10*, 21927–21938. [[CrossRef](#)]
162. Gisbert-Garzarán, M.; Manzano, M.; Vallet-Regí, M. Mesoporous silica nanoparticles for the treatment of complex bone diseases: Bone cancer, bone infection and osteoporosis. *Pharmaceutics* **2020**, *12*, 83. [[CrossRef](#)]
163. Moreira, A.F.; Dias, D.R.; Correia, I.J. Stimuli-responsive mesoporous silica nanoparticles for cancer therapy: A review. *Microporous Mesoporous Mater.* **2016**, *236*, 141–157. [[CrossRef](#)]
164. Slowing, I.; Viveroescoto, J.; Wu, C.; Lin, V. Mesoporous silica nanoparticles as controlled release drug delivery and gene transfection carriers. *Adv. Drug Deliv. Rev.* **2008**, *60*, 1278–1288. [[CrossRef](#)]
165. Parhi, P.; Mohanty, C.; Sahoo, S.K. Nanotechnology-based combinational drug delivery: An emerging approach for cancer therapy. *Drug Discov. Today* **2012**, *17*, 1044–1052. [[CrossRef](#)]
166. Tang, F.; Li, L.; Chen, D. Mesoporous silica nanoparticles: Synthesis, biocompatibility and drug delivery. *Adv. Mater.* **2012**, *24*, 1504–1534. [[CrossRef](#)] [[PubMed](#)]
167. Kumari, A.; Yadav, S.K.; Yadav, S.C. Biodegradable polymeric nanoparticles based drug delivery systems. *Colloids Surf. B Biointerfaces* **2010**, *75*, 1–18. [[CrossRef](#)] [[PubMed](#)]

168. Teo, J.Y.; Chin, W.; Ke, X.; Gao, S.; Liu, S.; Cheng, W.; Hedrick, J.L.; Yang, Y.Y. pH and redox dual-responsive biodegradable polymeric micelles with high drug loading for effective anticancer drug delivery. *Nanomed. Nanotechnol. Biol. Med.* **2017**, *13*, 431–442. [[CrossRef](#)] [[PubMed](#)]
169. Phillips, D.J.; Gibson, M.I. Redox-sensitive materials for drug delivery: Targeting the correct intracellular environment, tuning release rates, and appropriate predictive systems. *Antioxidants Redox Signal.* **2014**, *21*, 786–803. [[CrossRef](#)]
170. Baeza, A.; Colilla, M.; Vallet-Regí, M. Advances in mesoporous silica nanoparticles for targeted stimuli-responsive drug delivery. *Expert Opin. Drug Deliv.* **2015**, *12*, 319–337. [[CrossRef](#)] [[PubMed](#)]
171. Sharafian, A.; Fayazmanesh, K.; McCague, C.; Bahrami, M. Thermal conductivity and contact resistance of mesoporous silica gel adsorbents bound with polyvinylpyrrolidone in contact with a metallic substrate for adsorption cooling system applications. *Int. J. Heat Mass Transf.* **2014**, *79*, 64–71. [[CrossRef](#)]
172. Chang, D.; Gao, Y.; Wang, L.; Liu, G.; Chen, Y.; Wang, T.; Tao, W.; Mei, L.; Huang, L.; Zeng, X. Polydopamine-based surface modification of mesoporous silica nanoparticles as pH-sensitive drug delivery vehicles for cancer therapy. *J. Colloid Interface Sci.* **2016**, *463*, 279–287. [[CrossRef](#)]
173. DeShong, P.R.; Zachariah, M.R.; DeMuth, P.; Prakash, A.; Luckett, C.; Stephen, D. Method for Forming Mesoporous Silica Nanoparticles, Mesoporous Silica Nanoparticles, and Applications Thereof. U.S. Patent No 9,271,936, 1 March 2016.
174. Ismail, O.H.; Ciogli, A.; Villani, C.; De Martino, M.; Pierini, M.; Cavazzini, A.; Bell, D.S.; Gasparri, F. Ultra-fast high-efficiency enantioseparations by means of a teicoplanin-based chiral stationary phase made on sub-2 $\mu$ m totally porous silica particles of narrow size distribution. *J. Chromatogr. A* **2016**, *1427*, 55–68. [[CrossRef](#)]
175. Knežević, N.Ž.; Durand, J.O. Large pore mesoporous silica nanomaterials for application in delivery of biomolecules. *Nanoscale* **2015**, *7*, 2199–2209. [[CrossRef](#)]
176. Casasús, R.; Marcos, M.D.; Martínez-Mañez, R.; Ros-Lis, J.V.; Soto, J.; Villaescusa, L.A.; Amorós, P.; Beltrán, D.; Guillem, C.; Latorre, J. Toward the Development of Ionically Controlled Nanoscopic Molecular Gates. *J. Am. Chem. Soc.* **2004**, *126*, 8612–8613. [[CrossRef](#)] [[PubMed](#)]
177. Song, S.W.; Hidajat, K.; Kawi, S. pH-Controllable drug release using hydrogel encapsulated mesoporous silica. *Chem. Commun.* **2007**, 4396. [[CrossRef](#)]
178. Hong, C.Y.; Li, X.; Pan, C.Y. Fabrication of smart nanocontainers with a mesoporous core and a pH-responsive shell for controlled uptake and release. *J. Mater. Chem.* **2009**, *19*. [[CrossRef](#)]
179. Angelos, S.; Yang, Y.W.; Patel, K.; Stoddart, J.F.; Zink, J.I. pH-Responsive Supramolecular Nanovalves Based on Cucurbit[6]uril Pseudorotaxanes. *Angew. Chem. Int. Ed.* **2008**, *47*, 2222–2226. [[CrossRef](#)] [[PubMed](#)]
180. Schroden, R.C.; Blanford, C.F.; Melde, B.J.; Johnson, B.J.S.; Stein, A. Direct Synthesis of Ordered Macroporous Silica Materials Functionalized with Polyoxometalate Clusters. *Chem. Mater.* **2001**, *13*, 1074–1081. [[CrossRef](#)]
181. Yang, Q.; Wang, S.; Fan, P.; Wang, L.; Di, Y.; Lin, K.; Xiao, F.S. pH-Responsive Carrier System Based on Carboxylic Acid Modified Mesoporous Silica and Polyelectrolyte for Drug Delivery. *Chem. Mater.* **2005**, *17*, 5999–6003. [[CrossRef](#)]
182. Juárez, L.A.; Añón, E.; Giménez, C.; Sancenón, F.; Martínez-Mañez, R.; Costero, A.M.; Gaviña, P.; Parra, M.; Bernardos, A. Self-Immolative Linkers as Caps for the Design of Gated Silica Mesoporous Supports. *Chem.-A Eur. J.* **2016**, *22*, 14126–14130. [[CrossRef](#)] [[PubMed](#)]
183. Chen, Y.; Yin, Q.; Ji, X.; Zhang, S.; Chen, H.; Zheng, Y.; Sun, Y.; Qu, H.; Wang, Z.; Li, Y.; et al. Manganese oxide-based multifunctionalized mesoporous silica nanoparticles for pH-responsive MRI, ultrasonography and circumvention of MDR in cancer cells. *Biomaterials* **2012**, *33*, 7126–7137. [[CrossRef](#)]
184. Cui, L.; Lin, H.; Guo, W.; Xiang, D.; Zhou, D.; Zhang, T.; Qu, F. A novel pH-responsive controlled release system based on mesoporous silica coated with hydroxyapatite. *J. Sol-Gel Sci. Technol.* **2014**, *72*, 106–113. [[CrossRef](#)]
185. Muhammad, F.; Guo, M.; Qi, W.; Sun, F.; Wang, A.; Guo, Y.; Zhu, G. PH-triggered controlled drug release from mesoporous silica nanoparticles via intracellular dissolution of ZnO nanolids. *J. Am. Chem. Soc.* **2011**, *133*, 8778–8781. [[CrossRef](#)]
186. Chen, X.; Qian, H.; Qiao, H.; Dong, B.; Chen, E.; Huang, D.; Wang, T.; Chen, W. Tumor-Adhesive and pH-Degradable Microgels by Microfluidics and Photo-Cross-Linking for Efficient Antiangiogenesis and Enhanced Cancer Chemotherapy. *Biomacromolecules* **2020**, *21*, 1285–1294. [[CrossRef](#)] [[PubMed](#)]

187. Chen, M.; Hu, J.; Wang, L.; Li, Y.; Zhu, C.; Chen, C.; Shi, M.; Ju, Z.; Cao, X.; Zhang, Z. Targeted and redox-responsive drug delivery systems based on carbonic anhydrase IX-decorated mesoporous silica nanoparticles for cancer therapy. *Sci. Rep.* **2020**, *10*. [[CrossRef](#)] [[PubMed](#)]
188. Xiao, D.; Hu, J.J.; Zhu, J.Y.; Wang, S.B.; Zhuo, R.X.; Zhang, X.Z. A redox-responsive mesoporous silica nanoparticle with a therapeutic peptide shell for tumor targeting synergistic therapy. *Nanoscale* **2016**, *8*, 16702–16709. [[CrossRef](#)]
189. Luo, Z.; Cai, K.; Hu, Y.; Zhao, L.; Liu, P.; Duan, L.; Yang, W. Mesoporous Silica Nanoparticles End-Capped with Collagen: Redox-Responsive Nanoreservoirs for Targeted Drug Delivery. *Angew. Chem. Int. Ed.* **2011**, *50*, 640–643. [[CrossRef](#)]
190. Xu, H.; Cao, W.; Zhang, X. Selenium-Containing Polymers: Promising Biomaterials for Controlled Release and Enzyme Mimics. *Acc. Chem. Res.* **2013**, *46*, 1647–1658. [[CrossRef](#)]
191. Lin, C.; Engbersen, J.F. The role of the disulfide group in disulfide-based polymeric gene carriers. *Expert Opin. Drug Deliv.* **2009**, *6*, 421–439. [[CrossRef](#)]
192. de la Torre, C.; Mondragón, L.; Coll, C.; Sancenón, F.; Marcos, M.D.; Martínez-Mañez, R.; Amorós, P.; Pérez-Payá, E.; Orzáez, M. Cathepsin-B Induced Controlled Release from Peptide-Capped Mesoporous Silica Nanoparticles. *Chem. A Eur. J.* **2014**, *20*, 15309–15314. [[CrossRef](#)] [[PubMed](#)]
193. Zheng, F.; Zhang, P.; Xi, Y.; Huang, K.; Min, Q.; Zhu, J.J. Peptide-mediated core/satellite/shell multifunctional nanovehicles for precise imaging of cathepsin B activity and dual-enzyme controlled drug release. *NPG Asia Mater.* **2017**, *9*. [[CrossRef](#)]
194. Chen, Z.; Li, Z.; Lin, Y.; Yin, M.; Ren, J.; Qu, X. Bioresponsive Hyaluronic Acid-Capped Mesoporous Silica Nanoparticles for Targeted Drug Delivery. *Chem.-A Eur. J.* **2013**, *19*, 1778–1783. [[CrossRef](#)]
195. Bernardos, A.; Aznar, E.; Marcos, M.D.; Martínez-Mañez, R.; Sancenón, F.; Soto, J.; Barat, J.M.; Amorós, P. Enzyme-Responsive Controlled Release Using Mesoporous Silica Supports Capped with Lactose. *Angew. Chem. Int. Ed.* **2009**, *48*, 5884–5887. [[CrossRef](#)] [[PubMed](#)]
196. Papat, A.; Ross, B.P.; Liu, J.; Jambhrunkar, S.; Kleitz, F.; Qiao, S.Z. Enzyme-Responsive Controlled Release of Covalently Bound Prodrug from Functional Mesoporous Silica Nanospheres. *Angew. Chem. Int. Ed.* **2012**, *51*, 12486–12489. [[CrossRef](#)] [[PubMed](#)]
197. Patel, K.; Angelos, S.; Dichtel, W.R.; Coskun, A.; Yang, Y.W.; Zink, J.I.; Stoddart, J.F. Enzyme-Responsive Snap-Top Covered Silica Nanocontainers. *J. Am. Chem. Soc.* **2008**, *130*, 2382–2383. [[CrossRef](#)] [[PubMed](#)]
198. Benival, D.M.; Devarajan, P.V. In Situ Lipidization as a New Approach for the Design of a Self Microemulsifying Drug Delivery System (SMEDDS) of Doxorubicin Hydrochloride for Oral Administration. *J. Biomed. Nanotechnol.* **2015**, *11*, 913–922. [[CrossRef](#)]
199. Zhao, Y.; Trewyn, B.G.; Slowing, I.I.; Lin, V.S.Y. Mesoporous Silica Nanoparticle-Based Double Drug Delivery System for Glucose-Responsive Controlled Release of Insulin and Cyclic AMP. *J. Am. Chem. Soc.* **2009**, *131*, 8398–8400. [[CrossRef](#)]
200. Aznar, E.; Villalonga, R.; Giménez, C.; Sancenón, F.; Marcos, M.D.; Martínez-Mañez, R.; Díez, P.; Pingarrón, J.M.; Amorós, P. Glucose-triggered release using enzyme-gated mesoporous silica nanoparticles. *Chem. Commun.* **2013**, *49*, 6391–6393. [[CrossRef](#)] [[PubMed](#)]
201. Hei, M.; Wu, H.; Fu, Y.; Xu, Y.; Zhu, W. Phenylboronic acid functionalized silica nanoparticles with enlarged ordered mesopores for efficient insulin loading and controlled release. *J. Drug Deliv. Sci. Technol.* **2019**, *51*, 320–326. [[CrossRef](#)]
202. Geng, J.; Li, M.; Wu, L.; Chen, C.; Qu, X. Mesoporous Silica Nanoparticle-based H<sub>2</sub>O<sub>2</sub> Responsive Controlled-Release System Used for Alzheimer's Disease Treatment. *Adv. Healthc. Mater.* **2012**, *1*, 332–336. [[CrossRef](#)]
203. Guo, F.; Li, G.; Zhou, H.; Ma, S.; Guo, L.; Liu, X. Temperature and H<sub>2</sub>O<sub>2</sub>-operated nano-valves on mesoporous silica nanoparticles for controlled drug release and kinetics. *Colloids Surf. B Biointerfaces* **2020**, *187*. [[CrossRef](#)]
204. Zhu, C.L.; Lu, C.H.; Song, X.Y.; Yang, H.H.; Wang, X.R. Bioresponsive Controlled Release Using Mesoporous Silica Nanoparticles Capped with Aptamer-Based Molecular Gate. *J. Am. Chem. Soc.* **2011**, *133*, 1278–1281. [[CrossRef](#)] [[PubMed](#)]
205. Fu, Q.; Rama Rao, G.V.; Ward, T.L.; Lu, Y.; Lopez, G.P. Thermoresponsive Transport through Ordered Mesoporous Silica/PNIPAAm Copolymer Membranes and Microspheres. *Langmuir* **2007**, *23*, 170–174. [[CrossRef](#)]

206. Mal, N.K.; Fujiwara, M.; Tanaka, Y. Photocontrolled reversible release of guest molecules from coumarin-modified mesoporous silica. *Nature* **2003**, *421*, 350–353. [[CrossRef](#)] [[PubMed](#)]
207. Kobayashi, H.; Turkbey, B.; Watanabe, R.; Choyke, P.L. Cancer Drug Delivery: Considerations in the Rational Design of Nanosized Bioconjugates. *Bioconjug. Chem.* **2014**, *25*, 2093–2100. [[CrossRef](#)] [[PubMed](#)]
208. Karthik, S.; Prashanth Kumar, B.N.; Gangopadhyay, M.; Mandal, M.; Singh, N.D.P. A targeted, image-guided and dually locked photoresponsive drug delivery system. *J. Mater. Chem. B* **2015**, *3*, 728–732. [[CrossRef](#)] [[PubMed](#)]
209. Liu, J.; Bu, J.; Bu, W.; Zhang, S.; Pan, L.; Fan, W.; Chen, F.; Zhou, L.; Peng, W.; Zhao, K.; et al. Real-Time In Vivo Quantitative Monitoring of Drug Release by Dual-Mode Magnetic Resonance and Upconverted Luminescence Imaging. *Angew. Chem. Int. Ed.* **2014**, *53*, 4551–4555. [[CrossRef](#)] [[PubMed](#)]
210. Park, C.; Lee, K.; Kim, C. Photoresponsive Cyclodextrin-Covered Nanocontainers and Their Sol-Gel Transition Induced by Molecular Recognition. *Angew. Chem. Int. Ed.* **2009**, *48*, 1275–1278. [[CrossRef](#)]
211. Chang, Y.T.; Liao, P.Y.; Sheu, H.S.; Tseng, Y.J.; Cheng, F.Y.; Yeh, C.S. Near-Infrared light-responsive intracellular drug and siRNA release using Au nanoensembles with oligonucleotide-capped silica shell. *Adv. Mater.* **2012**, *24*, 3309–3314. [[CrossRef](#)]
212. Yang, G.; Sun, X.; Liu, J.; Feng, L.; Liu, Z. Light-Responsive, Singlet-Oxygen-Triggered On-Demand Drug Release from Photosensitizer-Doped Mesoporous Silica Nanorods for Cancer Combination Therapy. *Adv. Funct. Mater.* **2016**, *26*, 4722–4732. [[CrossRef](#)]
213. Tao, C.; Zhu, Y. Magnetic mesoporous silica nanoparticles for potential delivery of chemotherapeutic drugs and hyperthermia. *Dalton Trans.* **2014**, *43*, 15482–15490. [[CrossRef](#)]
214. Abbasi, A.; Farooq, W.; Ali, N.; Ahmad, I. Simultaneous Effects of Brownian Motion, Thermophoresis and Curvature on Peristaltic Flow of an Oldroyd 4-Constant Fluid. *J. Nanofluids* **2019**, *8*, 736–745. [[CrossRef](#)]
215. Paris, J.L.; Cabañas, M.V.; Manzano, M.; Vallet-Regí, M. Polymer-Grafted Mesoporous Silica Nanoparticles as Ultrasound-Responsive Drug Carriers. *ACS Nano* **2015**, *9*, 11023–11033. [[CrossRef](#)]



© 2020 by the authors. Licensee MDPI, Basel, Switzerland. This article is an open access article distributed under the terms and conditions of the Creative Commons Attribution (CC BY) license (<http://creativecommons.org/licenses/by/4.0/>).